Article

Cell

LRRC8 Proteins Form Volume-Regulated Anion Channels that Sense Ionic Strength

Graphical Abstract

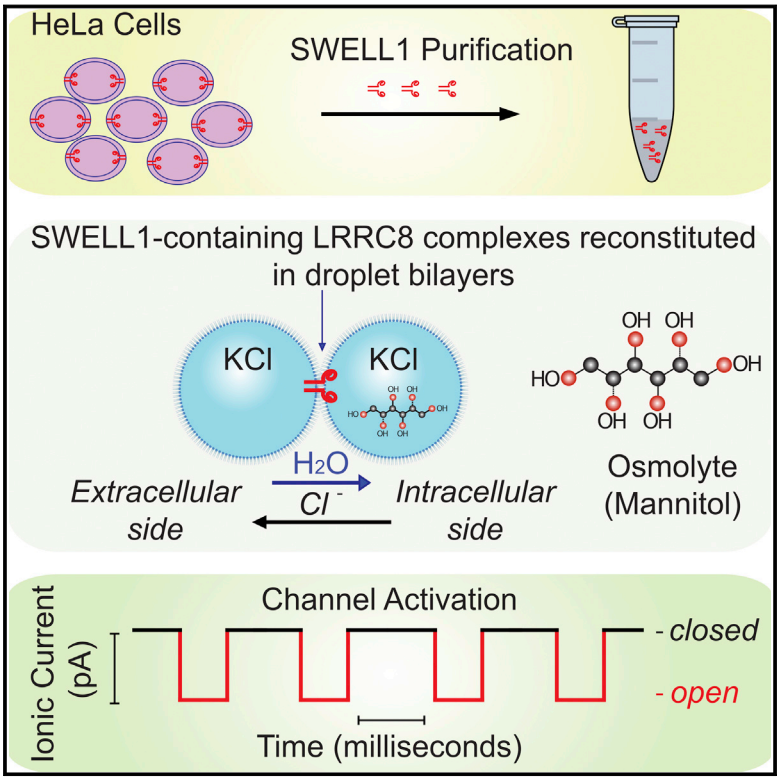

Authors

Ruhma Syeda, Zhaozhu Qiu, Adrienne E. Dubin, ..., Eric C. Peters, Mauricio Montal, Ardem Patapoutian

Correspondence

adubin@scripps.edu (A.E.D.), ardem@scripps.edu (A.P.)

In Brief

Analysis of the composition and regulatory mechanism of the volume-regulated anion channel (VRAC) reveals that it is formed from multiple LRRC8 subunits whose composition determines pore properties and encodes a sensor of ionic strength.

Highlights

- A complex of LRRC8 family proteins is sufficient to form the VRAC pore
- These channels are gated by osmotic disequilibrium in a minimalistic bilayer system
- LRRC8 subunits dictate VRAC single-channel γ, rectification, and anion selectivity
- Low ionic strength activates purified LRRC8 complex

Syeda et al., 2016, Cell *164*, 499–511
January 28, 2016
http://dx.doi.org/10.1016/j.cell.2015.12.031

CellPress

Article

Cell

LRRC8 Proteins Form Volume-Regulated Anion Channels that Sense Ionic Strength

Ruhma Syeda,[1,4] Zhaozhu Qiu,[1,2,4] Adrienne E. Dubin,[1,*] Swetha E. Murthy,[1] Maria N. Florendo,[1] Daniel E. Mason,[2] Jayanti Mathur,[2] Stuart M. Cahalan,[1] Eric C. Peters,[2] Mauricio Montal,[3] and Ardem Patapoutian[1,*]

[1]Department of Molecular and Cellular Neuroscience, Howard Hughes Medical Institute, Dorris Neuroscience Center, The Scripps Research Institute, La Jolla, CA 92037, USA

[2]Genomics Institute of the Novartis Research Foundation (GNF), San Diego, CA 92121, USA

[3]Division of Biological Sciences, University of California, San Diego, La Jolla, CA 92093, USA

[4]Co-first author

*Correspondence: adubin@scripps.edu (A.E.D.), ardem@scripps.edu (A.P.)

http://dx.doi.org/10.1016/j.cell.2015.12.031

SUMMARY

The volume-regulated anion channel (VRAC) is activated when a cell swells, and it plays a central role in maintaining cell volume in response to osmotic challenges. SWELL1 (LRRC8A) was recently identified as an essential component of VRAC. However, the identity of the pore-forming subunits of VRAC and how the channel is gated by cell swelling are unknown. Here, we show that SWELL1 and up to four other LRRC8 subunits assemble into heterogeneous complexes of ~800 kDa. When reconstituted into bilayers, LRRC8 complexes are sufficient to form anion channels activated by osmolality gradients. In bilayers, as well as in cells, the single-channel conductance of the complexes depends on the LRRC8 composition. Finally, low ionic strength (Γ) in the absence of an osmotic gradient activates the complexes in bilayers. These data demonstrate that LRRC8 proteins together constitute the VRAC pore and that hypotonic stress can activate VRAC through a decrease in cytoplasmic Γ.

INTRODUCTION

The ability to maintain constant cell volume is fundamental to cell function. Osmotically swollen cells restore their original volume and protect themselves via a process called regulatory volume decrease (RVD). This tightly controlled RVD is achieved by the activation of swelling-activated ion channels and K^+Cl^- co-transporters mediating ion and osmolyte efflux together with osmotically obligated water. Swelling-activated chloride currents ($I_{Cl,swell}$), mediated by a volume-regulated anion channel (VRAC), have been observed in nearly every vertebrate cell type, including lymphocytes, neurons, astrocytes, cardiac myocytes, and endothelial cells (Akita and Okada, 2014; Hoffmann et al., 2009; Pedersen et al., 2015).

LRRC8A (also named "SWELL1") was recently shown to be an essential component of VRAC since knockdown or deletion of SWELL1 abolished $I_{Cl,swell}$ (Qiu et al., 2014; Voss et al., 2014). SWELL1 (LRRC8A) is conserved across vertebrate species, and four additional homologous family members (LRRC8B-E) are usually present in their genomes (Abascal and Zardoya, 2012; Kubota et al., 2004). Deletion and rescue studies have shown that VRAC requires SWELL1 and at least one other LRRC8 subunit for function (Voss et al., 2014). Co-expression of LRRC8 subunits in heterologous systems has revealed subunit interactions by co-immunoprecipitation (Lee et al., 2014; Voss et al., 2014). A scanning cysteine mutagenesis approach identified the residue threonine 44 (T44) just external to the predicted transmembrane domain 1 of SWELL1, which, when mutated, altered the relative preference for two anions (I^- and Cl^-), suggesting that SWELL1 is in close proximity (or part) of the pore (Qiu et al., 2014). The extent of VRAC inactivation at positive voltages was subunit dependent, suggesting that LRRC8 proteins are likely associated with the channel (Voss et al., 2014). A recent report revealing subunit-specific effects on taurine flux is consistent with LRRC8C-E contributing to the pore (Planells-Cases et al., 2015). These studies indicate that VRAC is composed of at least two subunits that are part of an anion-selective channel. However, SWELL1 overexpression caused decreased $I_{Cl,swell}$ (Qiu et al., 2014; Voss et al., 2014), and LRRC8 members, together with SWELL1, could not increase $I_{Cl,swell}$ above wild-type (WT) levels, suggesting that they may not be sufficient for VRAC activity. This raises questions on whether SWELL1/LRRC8s are pore-forming subunits and hints at the requirement for other limiting factors/proteins (Kunzelmann, 2015; Qiu et al., 2014; Voss et al., 2014).

The mechanisms by which VRAC is activated by cell swelling have been debated for decades. Water influx and subsequent swelling have multiple consequences that involve local decreases in ion concentrations and changes in macromolecule crowding (Zhou et al., 2008), alterations in plasma membrane domains (Trouet et al., 1999), potential changes in bilayer tension (Anishkin et al., 2014; Brohawn et al., 2014), alterations in cytoskeleton, and activation of second-messenger pathways, including kinases and phosphatases, among others (Hoffmann et al., 2009; Pedersen et al., 2015). Importantly, it is unknown whether VRAC itself contains a sensor for the adequate stimulus during swelling or whether gating requires other cellular

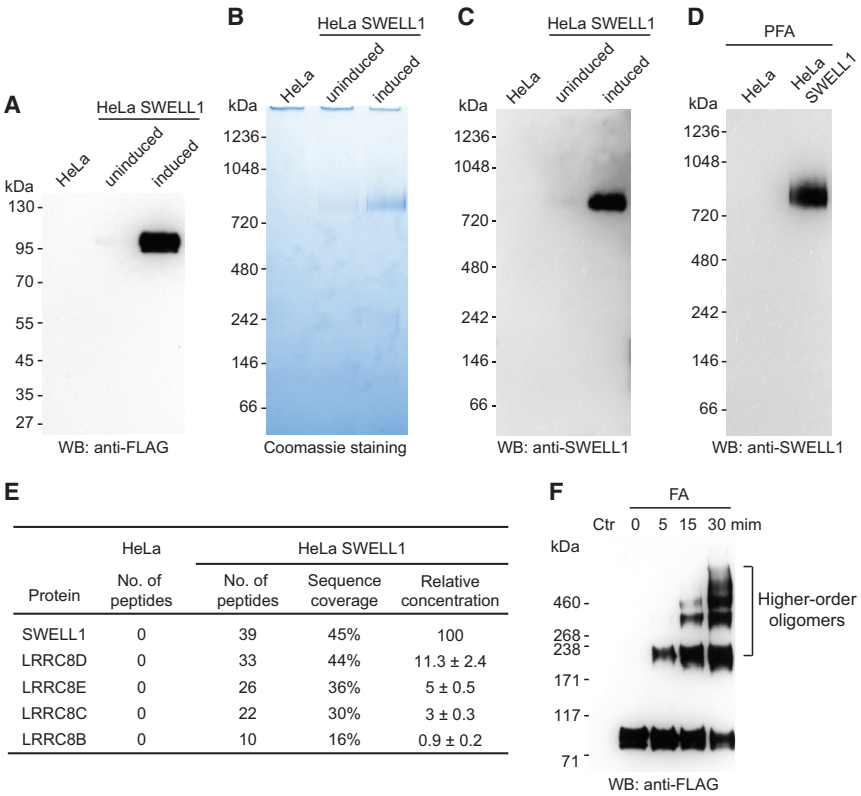

E

Protein	HeLa	HeLa SWELL1		
	No. of peptides	No. of peptides	Sequence coverage	Relative concentration
SWELL1	0	39	45%	100
LRRC8D	0	33	44%	11.3 ± 2.4
LRRC8E	0	26	36%	5 ± 0.5
LRRC8C	0	22	30%	3 ± 0.3
LRRC8B	0	10	16%	0.9 ± 0.2

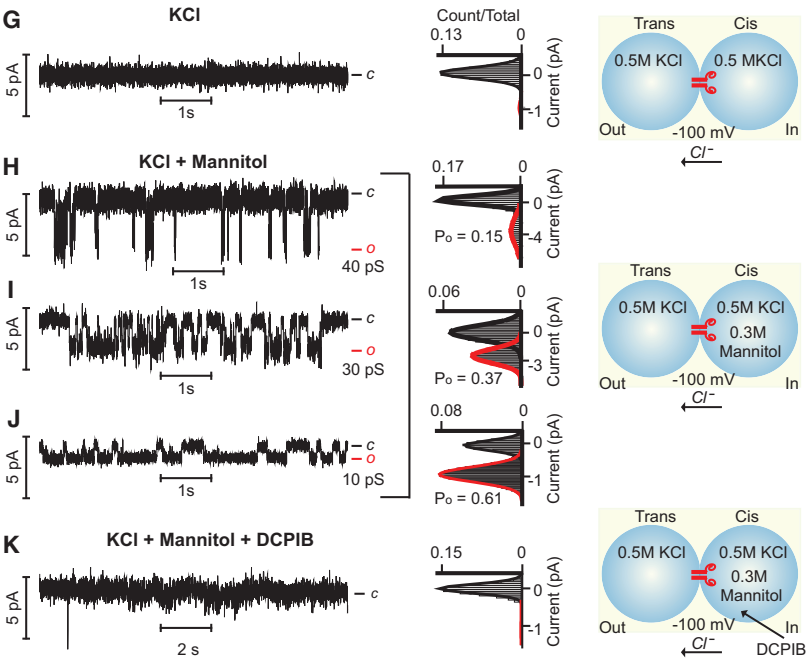

Figure 1. Purification and Reconstitution of SWELL1-Containing Protein Complexes

(A) Western blot (WB) showing SWELL1-FLAG expression in inducible HeLa cells at low TET concentration (5 ng/ml).

(B and C) Purified protein samples separated on native gels and visualized by Coomassie staining or western blotting with anti-SWELL1 antibody.

(D) WB of native gel separating proteins purified from paraformaldehyde (PFA)-treated cells.

(E) A representative mass spectrometry result identifying SWELL1 and its four homologs in the indicated purified protein samples. Relative protein concentrations observed in SWELL1-inducible HeLa cells were expressed as mean ± SEM (n = 3).

(F) Purified complexes treated with or without formaldehyde (FA) for the indicated time, separated on a denaturing gel and detected with anti-FLAG antibody. Ctr, control.

(G–J) Single-channel currents of reconstituted complexes in lipid bilayers at −100 mV and all-point current histograms for (G) isotonic (n = 15) and (H–J) hypotonic conditions generated by asymmetric mannitol (n > 30) as illustrated (right). Single-channel conductances (γ) in (H)–(J) are indicated below *o*.

(K) Blockade of currents after injection of DCPIB (40 μM final) into the *cis* droplet.

c and *o* indicate closed and open states, respectively.

See Figures S1, S2, and S3 and Tables S1 and S2.

components (e.g., cytoskeleton, enzymes, and second messengers). The most discussed mechanisms are increased membrane stress and disruption of cytoskeleton (Hoffmann et al., 2009; Nilius et al., 1996). Very few studies have addressed whether local changes in the ionic environment can stimulate gating (Cannon et al., 1998; Nilius et al., 1998). In the present study, we address two critical unsolved questions: what are the proteins that form the VRAC channel pore, and how does cell swelling lead to VRAC activation?

RESULTS

Biochemical Analysis of SWELL1-Containing Protein Complexes

To biochemically characterize SWELL1 (LRRC8A) and its associated proteins, we generated a HeLa cell line that could be induced to express SWELL1 tagged with FLAG at its carboxy-terminus (SWELL1-FLAG) (Figure 1A; Figure S1). SWELL1-FLAG rescued swelling-activated chloride currents ($I_{Cl,swell}$) in SWELL1 knockdown cells just like the WT gene (data not shown), suggesting that the tag has no obvious effect on SWELL1 function. Consistent with previous reports (Voss et al., 2014; Qiu et al., 2014), SWELL1 overexpression induced by high tetracycline (TET) concentrations (≥ 50 ng/ml) decreased $I_{Cl,swell}$ (Figure S1B). This inhibitory effect was not observed at low TET concentrations (5 and 10 ng/ml), which only increased SWELL1 mRNA expression within 2-fold above its endogenous level. We utilized

5 ng/ml TET for our biochemical experiments to ensure that ratios of SWELL1 and associated proteins were not considerably disrupted (uninduced cells expressed insufficient amounts of SWELL1-FLAG for biochemical studies; Figures 1A–1C). FLAG affinity purification from lysates of cells treated with 5 ng/ml TET revealed only one prominent protein band at ~800 kDa after native gel electrophoresis and Coomassie blue staining (Figure 1B). Western blots with an anti-SWELL1 antibody confirmed that this band contained SWELL1 (Figure 1C). To determine whether additional proteins might loosely interact with the ~800-kDa complex, we treated live cells with the crosslinker paraformaldehyde (PFA) before the purification procedure and found little or no detectable increase in the size of the SWELL1 protein complex on the native gel (Figure 1D versus Figures 1B and 1C).

LRRC8B, LRRC8C, LRRC8D, and LRRC8E each co-immunoprecipitates with SWELL1 in a heterologous overexpression system (Voss et al., 2014). To identify the proteins associated with SWELL1 in native complexes, we subjected the purified ~800-kDa band to mass spectrometry analysis and found that, in addition to SWELL1, many peptides derived from all four LRRC8 family members were detected (Figure 1E). No other specific interacting proteins were consistently observed, including known pore-forming ion channels (Table S1). Furthermore, mass spectrometry of the entire purified solution without gel separation revealed similar results (data not shown). These data indicate that, although it is possible that SWELL1 associates with other proteins in addition to its LRRC8 homologs, such an association might not be strong enough to withstand the FLAG affinity purification process. We refer to SWELL1 and its associated LRRC8 homologs as "SWELL1-containing complexes."

Next, we used the crosslinker formaldehyde (FA) to examine the oligomeric state of the subunits. FA-treated samples subjected to denaturing electrophoresis revealed at least five major bands in addition to larger unresolved molecular species (Figure 1F). The distribution of bands (consistent with increments of ~95 kDa, the predicted size of each subunit) suggests that they correspond to monomer, dimer, trimer, tetramer, pentamer, and potentially higher order oligomers. LRRC8 proteins are proposed to form hexamers based on their homology with pannexins (Abascal and Zardoya, 2012). The ~800-kDa complex observed on native gels (Figures 1B–1D) would predict up to eight subunits per complex if only the primary sequence is considered. However, slow migration and overestimation of molecular masses are not uncommon for membrane protein complexes due to many factors, such as glycosylation (Voss et al., 2014) and bound detergent and lipid molecules, which can add up to 20% mass (Wittig et al., 2010). Considering the potential size overestimation, the actual mass of SWELL1-containing complexes may vary roughly between six to eight times the predicted molecular weight of single LRRC8 polypeptides, suggesting the presence of six to eight LRRC8 subunits per complex.

In an effort to address the stoichiometry of LRRC8 proteins in the purified complex, we used quantitative mass spectrometry with stable-isotope-labeled peptide standards (Table S2). Surprisingly, the relative concentration varied dramatically among each LRRC8 protein (Figure 1E), with SWELL1 being the most abundant and LRRC8B being the rarest. These data are consistent with the lack of a specific immutable combination of subunits in each complex. Thus, purified complexes appear to be a heterogeneous assortment of multimers composed of mainly SWELL1 in combination with other LRRC8 subunits.

Functional Reconstitution of SWELL1-Containing Complexes in Lipid Bilayers

To assess whether purified LRRC8 protein complexes can form functional channels consistent with mediating $I_{Cl,swell}$, we used a simple bilayer system amenable to challenge with osmotic stimuli. Protein was supplemented in the droplet attached to the commanding potential electrode termed *cis*, in the presence of ATP to block channels that may insert into the bilayer with extracellular domains exposed to the *cis* side (Jackson and Strange, 1995; Tsumura et al., 1996); the *trans* droplet was grounded. A hypotonic gradient was generated by supplementing 300 mM mannitol (*cis*) to cause water influx into this droplet (i.e., cytoplasmic side). Although we initially chose 500 mM KCl to enhance signal-to-noise and to resolve detailed features of single-channel currents, we found similar results using physiological osmolarities and salt concentrations (discussed later). Channel activity was not observed when the protein was reconstituted in isotonic solution (Figure 1G), whereas a spectrum of single-channel conductance (γ) ranging from ~10 pS to 50 pS at −100 mV and open probability (P_o) ranging from 0.1 to 0.6 were reproducibly observed when complexes were exposed to a hypotonic stimulus (examples are shown in Figures 1H–1J). Importantly, activity was observed only when mannitol was introduced asymmetrically in the *cis* droplet (Figures 1H–1J) but not when equal concentrations of mannitol were present in both *cis* and *trans* droplets (Figure S2A). To exclude the possibility that mannitol elicited activity by a mechanism distinct from osmotic disequilibrium, we tested whether sucrose could also stimulate activity. Distinct channel activity with a range of γ was observed when the hypotonic stimulus was generated by a sucrose gradient, indicating that mannitol is not specifically activating channel complexes (Figures S2B and S2C). To assess whether ATP is required for channel function, we performed reconstitution studies in the absence of ATP in both *cis* and *trans* droplets while maintaining the relevant hypotonic stimulus. ATP was not required for us to observe distinct channel activity (Figure S3A); however, our bilayer studies cannot address whether there is a higher propensity for inactive channels in the absence of ATP. The hypotonicity-induced channel activity was blocked by injection of a VRAC blocker 4-[(2-butyl-6,7-dichloro-2-cyclopentyl-2,3-dihydro-1-oxo-1*H*-inden-5-yl)oxy]butanoic acid (DCPIB) in either droplet (Figure 1K and data not shown).

To test whether the reconstituted channels retained ion selectivity, lipid bilayers were created with 500 mM potassium gluconate on both sides (Figure S3B). Hypotonicity-induced currents at −100 mV in 500 mM potassium gluconate were smaller in amplitude (ranging from ~0.4 to 0.8 pA) than those in 500 mM KCl solution (~1–5 pA), indicating the dependence of currents on the anion species (not K^+) and that channels are capable of fluxing gluconate to some extent. These experiments provide evidence that isolated SWELL1-containing complexes incorporated into lipid bilayers act as bona fide anionic channels induced by hypotonicity and are sensitive to DCPIB.

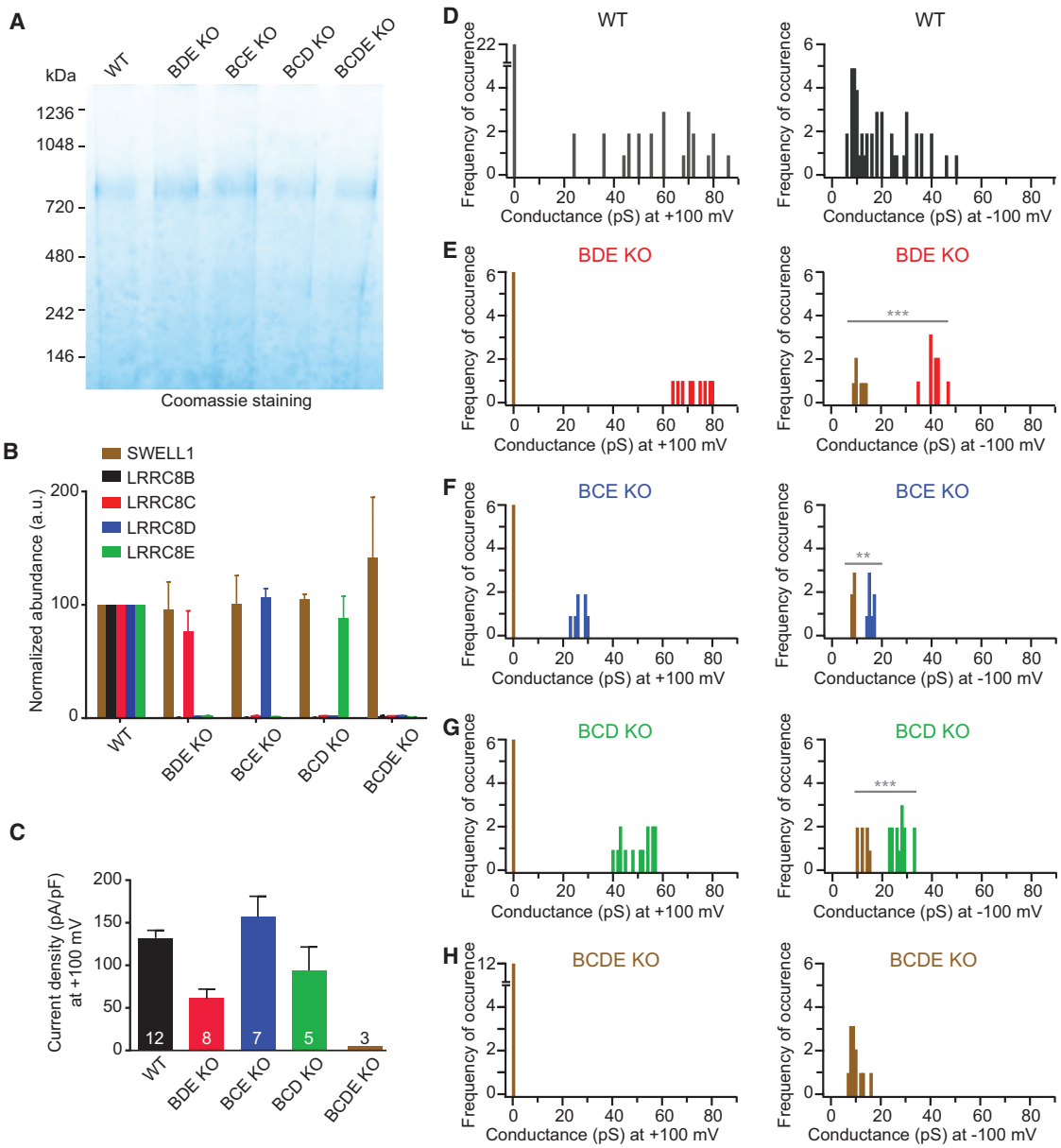

Figure 2. Purified LRRC8 Subunit Combinations Form Ion Channels with Distinct Channel Conductance in Droplet Lipid Bilayers

(A) Purified protein samples from WT and *LRRC8* triple (BDE, BCE, BCD)- and quadruple (BCDE)-KO SWELL1-inducible HeLa cells separated on a native gel and visualized by Coomassie staining.

(B) Abundance of each LRRC8 protein normalized to WT (mean ± SEM, n = 2) estimated by mass spectrometry.

(C) Whole-cell current densities of maximally activated $I_{Cl,swell}$ in WT and KO HeLa cells (mean ± SEM).

(D–H) Hypotonicity-induced single-channel conductance of reconstituted complexes after purification from (D) WT HeLa, (E–G) triple-KO HeLa, and (H) quadruple-KO HeLa cells (mean ± SEM, n = 2). At −100 mV, large conductance events were observed in samples from triple-KO cells that differed significantly from the small conductance events apparent in all samples, including those from quadruple-KO cells (brown bars) (**p < 0.01; ***p < 0.001, Student's t test). See Figure S4 and Table S3.

To address the specific role of various LRRC8 subunits in SWELL1-containing complexes, we constructed cell lines from which specific combinations of subunits can be purified. We focused on heteromers containing SWELL1 and only one other LRRC8 subunit. Specifically, we used clustered regularly interspaced short palindromic repeats (CRISPR)-Cas9 technology to disrupt multiple *LRRC8* genes in HeLa-inducible cells (Table S3). The purified SWELL1-containing complexes from triple and quadruple knockout (KO) cells migrated to the same position on a native gel as the sample from WT HeLa-inducible cells (Figure 2A). This indicates that the oligomeric state of SWELL1-containing complexes remains constant, despite the absence of

three or all four LRRC8 homologs. Mass spectrometry confirmed the predicted compositions of SWELL1-containing complexes purified from the various KO cell lines (Figure 2B). For example, the protein sample purified from *LRRC8(B/D/E)*$^{-/-}$ cells contained only SWELL1 and LRRC8C (Figure 2B, red bar). Next, we characterized $I_{Cl,swell}$ in KO cell lines (Figure 2C). Interestingly, whole-cell current densities in *LRRC8(B/C/E)*$^{-/-}$ and *LRRC8(B/C/D)*$^{-/-}$ cells were similar to those in WT cells, while *LRRC8(B/D/E)*$^{-/-}$ current densities were reduced by about half. In agreement with previous findings for human HCT116 cells (Voss et al., 2014), $I_{Cl,swell}$ was essentially not detected from *LRRC8(B/C/D/E)*$^{-/-}$ cells (Figure 2C), although homomeric SWELL1 complexes of ~800 kDa were observed (Figure 2A). These data confirm that SWELL1 and at least one other LRRC8 subunit are required for whole-cell VRAC activity.

A wide range of swelling-induced outwardly rectifying single-channel Cl^- conductances, all having the essential characteristics of VRAC, has been reported in cells (Nilius et al., 1996; Okada, 1997). In our droplet lipid bilayer experiments, SWELL1-containing complexes purified from WT cells also exhibited a broad γ range at both positive and negative voltages (Figures 1H–1J; Figure 2D). To test whether γ is determined by LRRC8 complex composition, we recorded single-channel currents of purified protein from KO cells expressing only two subunits. Remarkably, proteins purified from *LRRC8(B/D/E)*$^{-/-}$, *LRRC8(B/C/E)*$^{-/-}$, and *LRRC8(B/C/D)*$^{-/-}$ cells produced hypotonicity-induced channel activities with a more limited γ range compared to WT (Figures 2E–2G). For simplicity, we refer to protein complexes purified from *LRRC8(B/D/E)*$^{-/-}$, *LRRC8(B/C/E)*$^{-/-}$, and *LRRC8(B/C/D)*$^{-/-}$ cells as LRRC8 A+C, A+D, and A+E, respectively. The γ of LRRC8 A+C (Figure 2E, red), A+D (Figure 2F, blue), and A+E (Figure 2G, green) were calculated at both positive and negative voltages. The calculated γ values of LRRC8 A+C, A+D, and A+E differ significantly from each other and were all represented within the conductance spectrum observed for WT. These experiments provide evidence that each LRRC8 heteromeric complex exhibits a distinct γ range and that the WT sample contains mixtures of heteromers that produces the observed broad γ range.

Surprisingly, although $I_{Cl,swell}$ was not observed in *LRRC8(B/C/D/E)*$^{-/-}$ cells using the standard whole-cell voltage ramp protocol, SWELL1-containing complexes purified from these cells produced DCPIB-sensitive hypotonicity-induced currents at −100 mV, but not 100 mV, in lipid bilayers (Figure 2H; Figure S4). The discrepancy between whole-cell and lipid bilayer current recordings for SWELL1 homomers is not currently understood. Technical limitations may prohibit the study of homomers at 100 mV, since only steady-state current activity is measured in the lipid bilayers. Based on the results from triple and quadruple KO samples, we assign the populations with smallest γ at −100 mV to SWELL1 homomers (Figure 2H, brown; 8–16 pS) that significantly differs from the γ range of heteromeric LRRC8 A+C (35–47 pS), A+D (14–19 pS), and A+E (23–33 pS) complexes at −100 mV (Figures 2E–2G). These results suggest that SWELL1 homomers form stable channels in lipid bilayers (Figure 2H) and co-exist with heteromers composed of SWELL1 and other LRRC8 subunits (Figures 2D–2G). Importantly, channel activity recorded from the purified proteins indicates that the γ range is dependent on the identity of the LRRC8 subunit associating with SWELL1 in the complex. These experiments also rule out the possibility that a rare impurity, rather than a SWELL1-containing complex, accounts for the channel activities we observed.

LRRC8-Mediated Single-Channel Currents from Swollen HeLa Cells

Next, we validated the VRAC γ variability in native cells. We performed cell-attached patch clamp recordings from HeLa cells in isotonic (ISO) versus hypotonic (HYPO; 265 mOsm/kg) solution to identify VRAC-like single-channel events. Cells were bathed in high K^+ solutions to suppress RVD. We generated another panel of LRRC8 KO lines in WT HeLa cells (Table S4) and used *LRRC8(A/B/C/D/E)*$^{-/-}$ cells, which had essentially no $I_{Cl,swell}$, to confirm that any observed activity was, indeed, mediated by VRAC (data not shown). In HYPO solution, small single-channel currents were observed in ~50% of the *LRRC8(A/B/C/D/E)*$^{-/-}$ patches at positive potentials (resting potential [RP] + 100 mV) (mean ± SEM, 1.0 ± 0.07 pA, n = 20; Figure S5A). Similar activity was also observed when the cells were bathed in ISO solution (1.4 ± 0.3 pA, n = 5). These small conductance channels (~10 pS) were also observed in WT cells and had a similar incidence of occurrence, independent of swelling (in ISO: 0.98 ± 0.04 pA, n = 5; in HYPO: 1.0 ± 0.1 pA, n = 10; Figure S5B). Since these single-channel currents were independent of cell type and osmotic stimulus, any single-channel activity with amplitudes less than 1.7 pA (2 SD above the mean) was deemed as background. In addition to this background current, when WT cells were bathed in HYPO solution and cell-attached patches from swollen cells were made, larger amplitude, inactivating single-channel currents were observed at positive potentials. Importantly, these larger currents were not observed in *LRRC8(A/B/C/D/E)*$^{-/-}$ control cells. Single-channel currents from swollen WT HeLa cells revealed a pronounced heterogeneity in current amplitude from 1.8 pA to 7.3 pA at 100 mV above RP (Figure 3A). These types of currents were not observed in patches from WT cells in ISO solution (n = 5). To determine whether conductance depended on subunit composition, we tested *LRRC8(B/D/E)*$^{-/-}$ and *LRRC8(B/C/E)*$^{-/-}$ cells (Figures 3B and 3C). The corresponding LRRC8 A+C and A+D heteromers exhibited the largest and smallest conductances, respectively, in bilayers. Interestingly, *LRRC8(B/D/E)*$^{-/-}$ cells revealed single-channel currents with amplitudes from 3.1 to 6.4 pA (4.65 ± 0.18 pA, n = 22; Figure 3B), while *LRRC8(B/C/E)*$^{-/-}$ showed single-channel currents from 2.0 to 3.4 pA (2.48 ± 0.18 pA, n = 7; Figure 3C), a statistically significant difference (Student's t test, $p < 0.001$). Currents greater than 1.7 pA were not observed when cells were bathed in ISO solution (n = 12 and 10 for *LRRC8(B/D/E)*$^{-/-}$ and *LRRC8(B/C/E)*$^{-/-}$, respectively). Therefore, the cellular data corroborate the heterogeneity observed for reconstituted SWELL1-containing complexes in droplet lipid bilayers and underscore the importance of subunit composition to channel conductance.

LRRC8 Subunit Composition Dictates VRAC Rectification

One of the characteristic features of VRAC is its outward rectification, i.e., larger outward currents (Cl^- influx) than inward

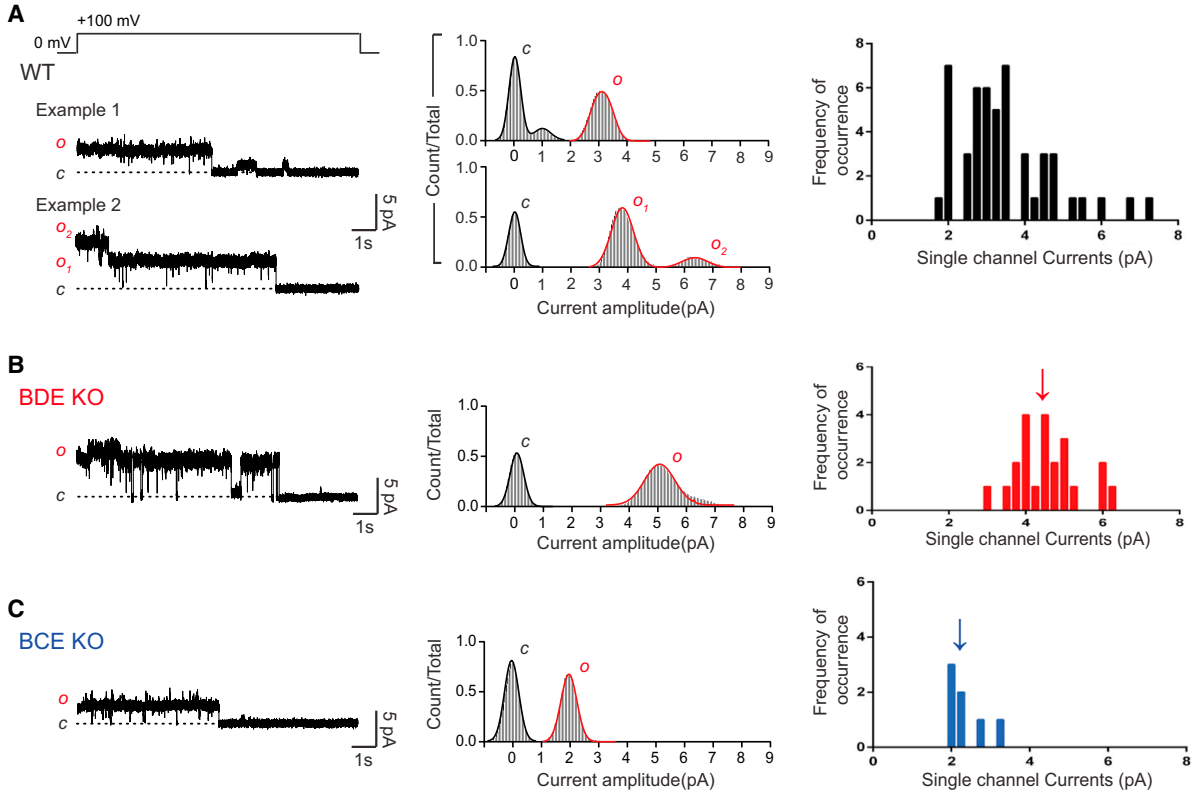

Figure 3. Single-Channel Currents in Cell-Attached Patches from Swollen HeLa Cells Reveal that Conductance Depends on Subunit Composition

(A–C) Representative single-channel traces (10 s, left) and all-point current histograms (middle) from WT (A), BDE KO (B), and BCE KO (C) cells recorded near 100 mV (pipette potential, −100 mV). Right: frequency distribution of current amplitudes observed in single patches from separate cells.

(A) A wide range of single-channel current amplitudes was observed from WT HeLa cells (n = 19, right) (Example 1: 3.0 pA; Example 2: 2.5 pA and 3.8 pA). Background channel activity was present in Example 1 (0.9 pA). Voltage protocol is indicated above.

(B) Current amplitude of channels composed of SWELL1 and LRRC8C was 4.6 ± 0.2 pA (mean [arrow] ± SEM, n = 22 from 11 patches).

(C) Current amplitude of channels composed of SWELL1 and LRRC8D was 2.5 ± 0.2 pA (mean [arrow] ± SEM, n = 7 from five patches).

See Figure S5 and Table S4.

currents (Cl^- efflux) at positive versus negative membrane potentials, respectively (Nilius et al., 1996; Pedersen et al., 2015). Single-channel analysis and all-points current histograms revealed that purified LRRC8 A+C, A+D, and A+E heteromers retained outward rectification in lipid bilayers (Figures 4A–4C). The currents at positive voltage were larger compared to currents at negative voltage for all complexes (Figures 4A–4C; Figure S6). To determine whether rectification properties depended on subunit composition, we analyzed the extent of single-channel rectification for both γ (Figures 4D–4F) and P_o (Figures 4G–4I). The ratio of γ observed at positive to negative potentials was the same for LRRC8 A+C, A+D, and A+E, suggesting that the extent of rectification due to γ is the same for all complexes tested (Figure 4F). Interestingly, the ratio of P_o acquired at 100 to that of −100 mV was significantly greater for LRRC8 A+D compared to LRRC8 A+C and LRRC8 A+E (Figure 4I). Remarkably, the outward rectification of $I_{Cl,swell}$ in whole-cell recordings of the triple KO cells mirrored that observed in lipid bilayers (Figures 4J–4K). The ratio of currents ($I_{outward}/I_{inward}$) recorded from *LRRC8(B/C/E)*$^{-/-}$ cells was larger compared to *LRRC8(B/D/E)*$^{-/-}$ and *LRRC8(B/C/D)*$^{-/-}$ cells (Figure 4K). Our single-channel data confirm previous findings that whole-cell rectification is, in part, due to differences in γ at positive versus negative potentials (Nilius et al., 1996). Bilayer studies suggest that P_o can also contribute to rectification in LRRC8D-containing heteromeric complexes. The inability to record for longer times from cell-attached patches on swollen cells at large positive potentials limited us from obtaining substantial data to determine accurate P_o values and, therefore, prohibited a direct comparison between bilayers and cells. Nonetheless, rectification properties depend on LRRC8 subunit composition.

LRRC8 Subunits Associating with SWELL1 Contribute to Ion Selectivity

Since it is generally agreed that channel conductance is a property of the pore, these bilayer data indicate that LRRC8C-E can contribute to pore properties of SWELL1-containing complexes. We next examined whether LRRC8 subunit composition alters the anion permeation properties of heteromeric complexes in

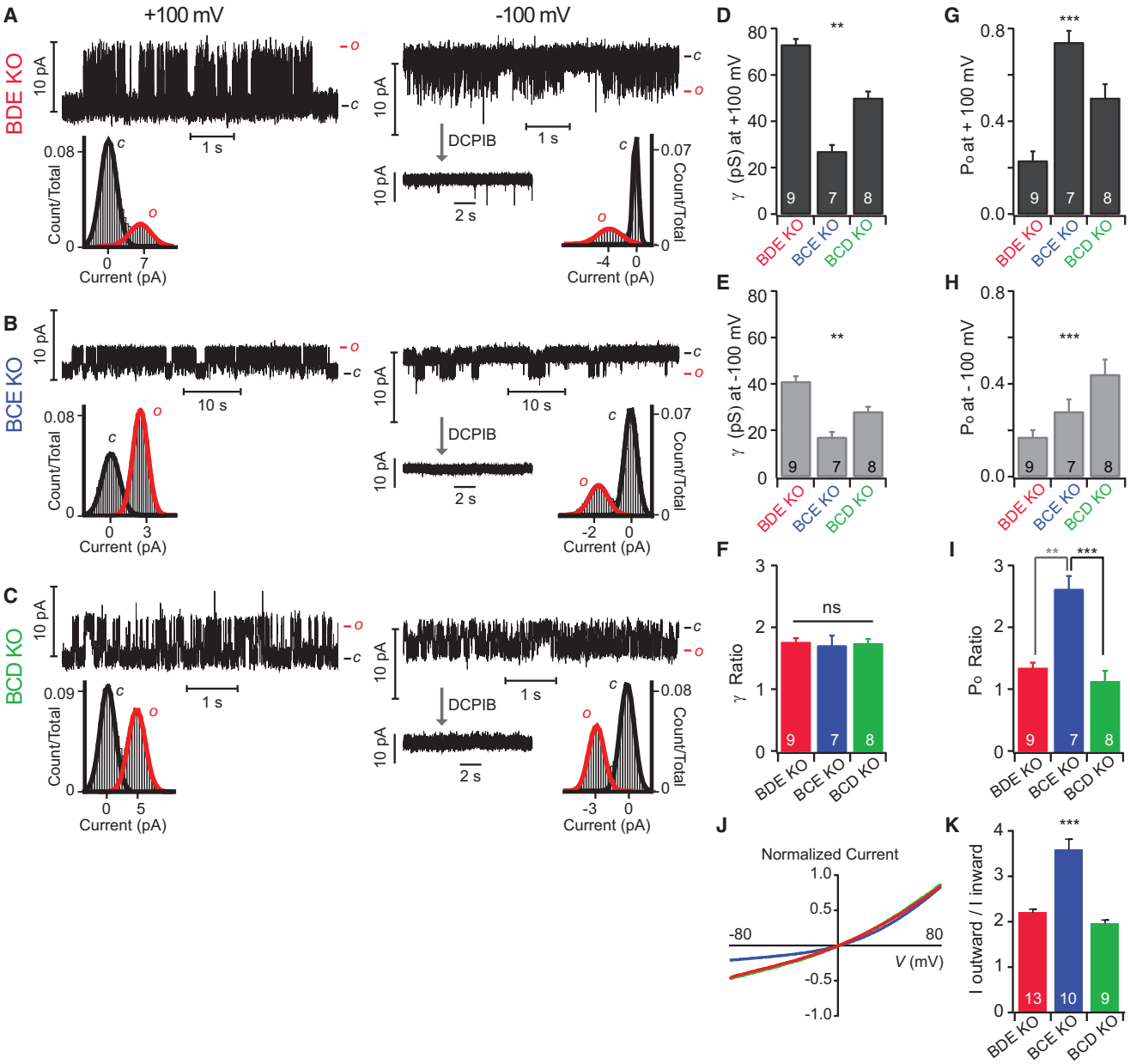

Figure 4. LRRC8 Subunit Combinations Determine VRAC Outward Rectification

(A–C) Single-channel recordings and all-point current histograms of SWELL1-containing complexes purified from the indicated *LRRC8* KO SWELL1-inducible HeLa cells. Inset: block by DCPIB injection (40 μM final) into the *cis* droplet.

(D–F) The γ of purified SWELL1-containing complexes and γ ratio (+V:−V).

(G–I) P_o and P_o ratio (+V:−V); $p < 0.01$ for A+C versus A+D and $p < 0.001$ for A+E versus A+D heteromers. P_o ratio for A+C versus A+E heteromers was not significantly different.

(J) Representative leak-subtracted whole-cell hypotonicity-induced currents for *LRRC8(B/D/E)*$^{-/-}$ (red), *LRRC8(B/C/E)*$^{-/-}$ (blue), and *LRRC8(B/C/D)*$^{-/-}$ (green) normalized to the maximum current at 100 mV and centered at V_{rev}.

(K) Ratio of whole-cell current at ±80mV from V_{rev} for the indicated cells reveals stronger outward rectification for $I_{Cl,swell}$ in BCE KO compared to other KO cells. Error bars indicate mean ± SEM. Significant differences (one-way ANOVA) are shown. **p < 0.01, and ***p < 0.001.

See Figure S6.

cells, another pore-related property. Our previous mutagenesis screen identified T44 as a critical residue of SWELL1, as cysteine replacement of this residue (T44C) significantly increased I^- versus Cl^- permeability (P_I/P_{Cl}). T44 is predicted to be located at the external boundary of TM1 and, intriguingly, is a conserved residue in the other LRRC8 subunits except LRRC8B. To

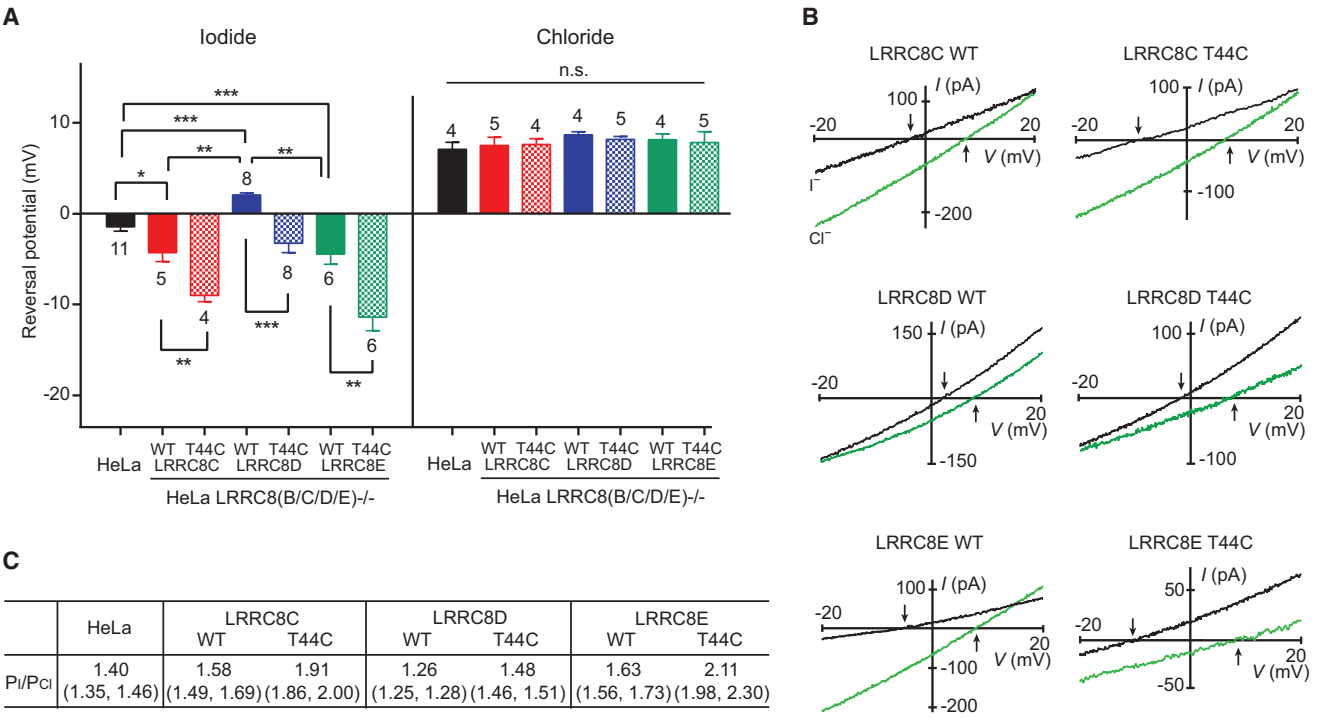

C

	HeLa	LRRC8C WT	LRRC8C T44C	LRRC8D WT	LRRC8D T44C	LRRC8E WT	LRRC8E T44C
P_I/P_{Cl}	1.40 (1.35, 1.46)	1.58 (1.49, 1.69)	1.91 (1.86, 2.00)	1.26 (1.25, 1.28)	1.48 (1.46, 1.51)	1.63 (1.56, 1.73)	2.11 (1.98, 2.30)

Figure 5. T44C Mutations in LRRC8 Subunits Alter Anion Selectivity

(A) V_{rev} for $I_{Cl,swell}$ recorded from parental or *LRRC8(B/C/D/E)*$^{-/-}$ HeLa cells expressing WT or T44C LRRC8 subunits was determined in the presence of I^- or Cl^- as the only extracellular anion. Bars represent mean ± SEM (*p < 0.05; **p < 0.01; ***p < 0.001; n.s., not significant; unpaired Student's t test).

(B) Representative leak-subtracted currents recorded in I^- (black) and Cl^- (green). More negative V_{rev} (arrows) in I^- versus Cl^- solutions indicates selectivity for I^- over Cl^-.

(C) P_I/P_{Cl} calculations based on data shown in (A); values in parentheses indicate the upper and lower compound SEM.

examine the effect of the same point mutation in LRRC8C-E subunits, we rescued $I_{Cl,swell}$ in *LRRC8(B/C/D/E)*$^{-/-}$ cells by transfecting either WT or T44C mutant LRRC8 cDNAs. The reversal potential (V_{rev}) of hypotonicity-induced currents was determined when I^- or Cl^- was the only permeant extracellular anion and P_I/P_{Cl} was calculated from the difference in V_{rev} as previously described (Qiu et al., 2014). While $I_{Cl,swell}$ in all cells reversed near E_{Cl} as expected, V_{rev} in the I^- solution for all T44C mutants was significantly shifted to more negative potentials compared to their corresponding WT controls (Figures 5A and 5B). This indicates that, like SWELL1 T44C, cysteine mutations at T44 in other LRRC8 subunits also enhance P_I/P_{Cl} (Figure 5C). Additionally, compared to native $I_{Cl,swell}$ in HeLa-inducible cells, VRAC currents rescued by WT LRRC8C or LRRC8E showed a significantly higher I^- selectivity, while WT LRRC8D revealed a reduced P_I/P_{Cl} (Figure 5). This suggests that LRRC8 subunits also affect VRAC I^- versus Cl^- selectivity in HeLa cells. Taken together, the γ and rectification properties in lipid bilayers and the finding that LRRC8 subunits and their point mutations contribute to anion selectivity demonstrate that LRRC8C-E proteins can contribute to the VRAC pore.

LRRC8 Protein Complexes Are Activated by Low Intracellular Ionic Strength

Permeation properties of $I_{Cl,swell}$ have been well studied (Akita and Okada, 2014; Pedersen et al., 2015), but the activation mechanism of VRAC at the molecular level is not understood. Hypotonicity-induced cell swelling and increase in the cell volume could evoke numerous physiologically relevant effects, including (1) mechanical changes in the cells, (2) alterations in cellular signaling, and (3) local decreases in the intracellular ion concentration due to water influx. Our protein purification and reconstitution approach excluded an essential role of cellular components and signaling pathways in the activation of SWELL1-containing complexes. Thus, we examined whether any of the remaining mechanisms, i.e., mechanical changes in the membrane or decreases in ionic strength (Γ), are essential for the activity of purified protein complexes in droplet lipid bilayers. To assess the activation mechanism based on volume increase and membrane stretch, LRRC8 A+C, A+D, and A+E heteromers were reconstituted in lipid bilayers under ISO conditions (500 mM KCl, 10 mM HEPES, pH 7.4), and 40 nl of this solution was injected into either the *cis* or *trans* droplet of the pre-formed bilayers. This injection resulted in ~20% increase in the droplet volume but did not evoke channel activity for any of the LRRC8 heteromers tested (n = 9; data not shown). This stimulus was, however, sufficient to activate mechanically activated MscS channels (data not shown) (Battle et al., 2009). This suggests that the increase in droplet volume and the subsequent mechanical changes in the lipid bilayer is not the likely cause of channel activity.

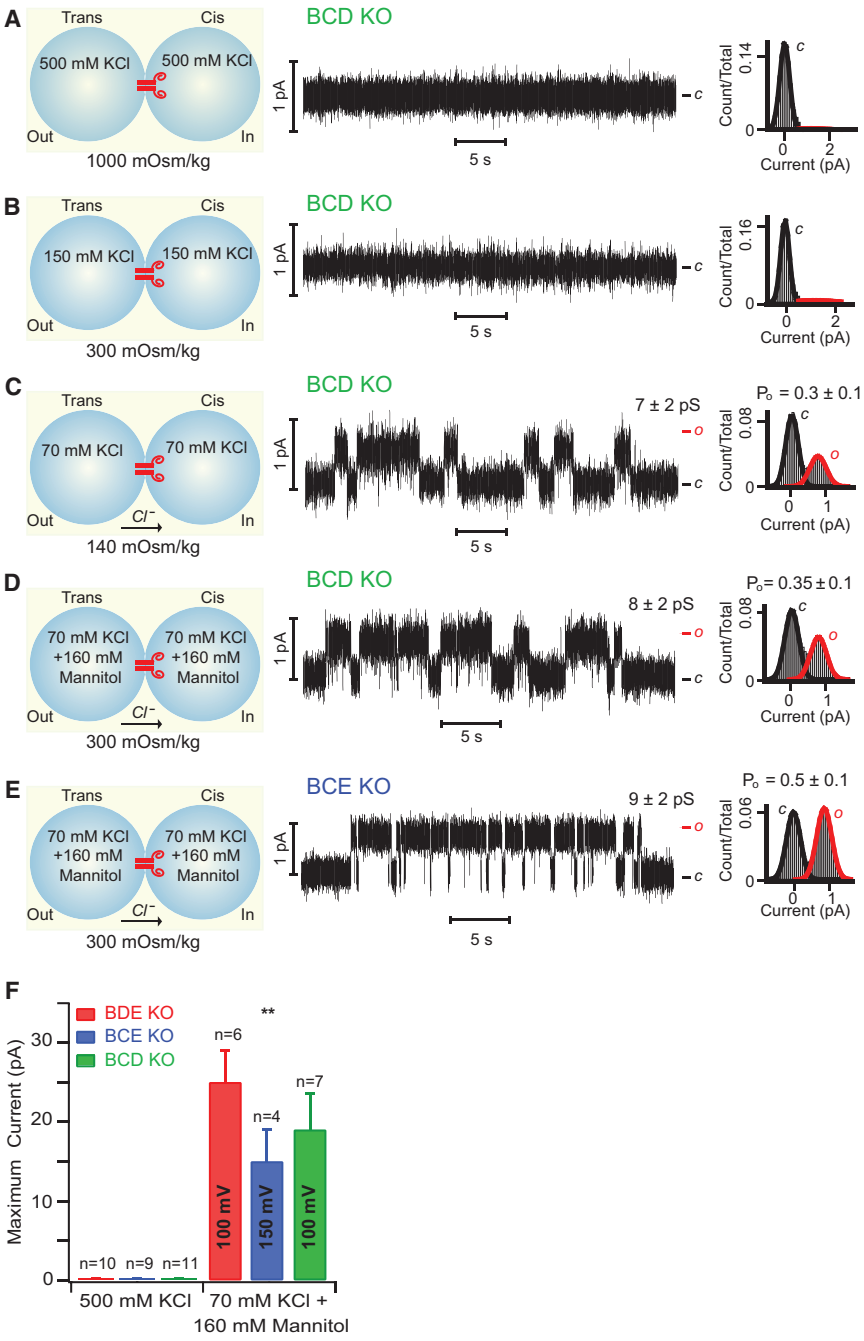

Figure 6. LRRC8 Proteins Are Activated by Low Ionic Strength

(A–C) Single-channel current recordings of the indicated SWELL1-containing complexes after reconstitution in lipid bilayers under different salt conditions (in millimolar): (A) 500 KCl (n = 6), (B) 150 KCl (n = 8), and (C) 70 KCl (n = 7).

(D and E) Single-channel currents in 70 mM KCl and mannitol to adjust to physiological osmolality (~300 mOsm/kg) (n = 6 and 8 for D and E, respectively).

(F) Maximum currents from multi-channel recordings of indicated complexes in low Γ (n > 15). Error bars indicate means ± SEM.

All data were acquired at 100 mV except for (E, 150 mV). Significant differences were observed in low Γ for all groups (one-way ANOVA); **p < 0.01. γ and P_o presented in (C)–(E) are means ± SEM.

Next, we screened the effect of low Γ on the activation of SWELL1-containing complexes. Three different salt concentrations were tested in the lipid bilayers: 500 mM KCl to represent high Γ (standard solution for droplet bilayer recordings), 150 mM KCl to represent physiological Γ, and 70 mM KCl to represent low Γ. Channel activity was not observed when LRRC8 A+C, A+D, and A+E heteromers were reconstituted in droplet lipid bilayers established from *cis* and *trans* droplets containing 500 (Figure 6A) or 150 mM KCl (Figure 6B, examples shown for LRRC8 A+E). However, robust currents exhibiting γ = 8 ± 2 pS (Figure 6C) were recorded from reconstituted LRRC8 A+E heteromers in symmetric 70 mM KCl. Since decreasing the Γ from physiological 150 mM KCl to low 70 mM KCl also decreases osmolality of the solution from ~300 mOsm/kg to ~140 mOsm/kg, we tested whether channel activity in 70 mM KCl was due to decreased Γ or decreased osmolality. LRRC8 A+E activity was still observed when osmolality was kept at physiological levels by supplementing 160 mM mannitol while decreasing Γ to 70 mM KCl (Figure 6D), indicating that the protein complex can be activated by lowering the Γ in the absence of an osmotic gradient. Discrete single-channel currents were recorded that exhibited a γ of 8 ± 2 pS, comparable to channel properties observed in the isotonic 70 mM KCl solution (Figures 6C and 6D). LRRC8 A+C and A+D activity was also reproducibly observed in isotonic 70 mM KCl (Figures 6E and 6F) but not in 150 or 500 mM KCl (Figure 6F). Regardless of the combination of LRRC8 heteromers, all SWELL1-containing complexes tested produced DCPIB-sensitive currents in droplet bilayers under low Γ conditions (data not shown). These data indicate that SWELL1-containing complexes are activated by lowering the Γ in a minimalistic bilayer system.

DISCUSSION

VRAC is activated during shifts in osmotic homeostasis that lead to cell swelling and contributes to a variety of physiological and pathophysiological processes (Akita and Okada, 2014; Hoffmann et al., 2009; Kunzelmann, 2015). Here, we take advantage

of our recent identification of SWELL1 (Qiu et al., 2014) as an essential component of VRAC to purify and characterize SWELL1-containing complexes. We gained three fundamental insights using a combination of biochemical and electrophysiological methods. First, VRAC is a heterogeneous collection of high-molecular-weight (~800 kDa) complexes composed of LRRC8 proteins, which, when purified and incorporated in lipid bilayers, can be directly activated by an osmotic gradient. Second, SWELL1 and LRRC8C-E subunits together are sufficient to make pore-forming ion channels; channel conductance, permeability, and rectification depend on the nature of the associating non-SWELL1 LRRC8 protein. Third, low Γ directly gates VRAC in a minimalistic bilayer system, giving us a mechanistic insight on how VRAC is gated in response to cell swelling. This finding also indicates that VRAC opening does not require other cellular components and that the sensor is encoded within the channel complex.

VRAC Is a Heterogeneous Collection of Ion Channels Composed of LRRC8 Proteins

By immunoprecipitating SWELL1 from HeLa cells, we identified all other members of LRRC8 family (LRRC8B-E) but no other proteins, specifically associating with SWELL1 in an ~800-kDa native complex. Interestingly, the ratio of associating proteins was not consistent with the existence of a single entity. However, the number of subunits per pore-forming complex appears to be constant, regardless of subunit composition. Given the homology of LRRC8 proteins to pannexin (Abascal and Zardoya, 2012), their predicted unmodified molecular weights (~95 kDa), and their likelihood of being glycosylated (Voss et al., 2014), LRRC8 subunits probably assemble as hexameric channels. SWELL1 is an obligatory subunit in this complex (Qiu et al., 2014; Voss et al., 2014), and at least one of the other four LRRC8 homologs is required (Figure 2; Voss et al., 2014). Furthermore, the exact stoichiometry and intramolecular arrangement of SWELL1 and other LRRC8 subunits within the pore-forming complex are still unknown, and the anticipated flexibility in stoichiometry and arrangement suggests the existence of a very large cohort of disparate VRAC channels. Given the complexity, future single-molecule and structural studies are required to determine the stoichiometry and oligomeric state of LRRC8 heteromers. Several ligand-gated ion channel families exhibit similar flexibilities in subunit composition and their arrangement (Hille, 2001). However, this structural diversity with its consequential functional diversity in channel biophysical properties makes VRAC unique among ion channels.

Specific LRRC8 Subunits Associate with SWELL1 to Dictate Channel Properties

An intermediate γ range for VRAC has been described among different tissues and cells over the past 3 decades (Nilius et al., 1996; Okada, 1997). Although the currents were swelling dependent, the early studies suffered from a lack of molecular identity of VRAC and specific pharmacological tools. Furthermore, the underlying causes of this heterogeneity were not known.

The identification of the LRRC8 gene family as essential components of VRAC enabled us, with certainty, to identify LRRC8-dependent swelling-induced single-channel currents in cellular assays. Cell-attached patches from swollen HeLa cells revealed a wide range of current amplitudes. Although most early studies using cell-attached patches did not comment on current amplitude heterogeneity (Okada et al., 1994; Weiss and Lang, 1992), one study reported channels with at least two significantly different conductances with features of $I_{Cl,swell}$ (e.g., run down, inactivation at positive voltages) (Solc and Wine, 1991). Our single-channel studies conducted in droplet lipid bilayers also demonstrated the conductance heterogeneity of LRRC8 proteins. Outward single-channel currents in WT HeLa cells revealed a wide γ range from 18 to 73 pS at 100 mV (assuming an RP of 0 mV). However, when cells expressed only two of the five subunits, *LRRC8(B/D/E)*$^{-/-}$ and *LRRC8(B/C/E)*$^{-/-}$, the γ range became narrow and non-overlapping, similar to those observed in the lipid bilayers. The γ values obtained from swollen HeLa cells recorded in ~100 mM Cl^- lie between those observed in lipid bilayers formed in the presence of either 70 mM or 500 mM Cl^-. Regardless of the assay, the conductance of purified complexes reconstituted into lipid bilayers and VRAC expressed in cellular membranes depend on the identity of the associating subunit (LRRC8C-E). Consistent with previous reports (Nilius et al., 1996; Okada, 1997), single-channel currents from all combinations tested revealed similar rectification, where outward is greater than inward current in both cellular and lipid bilayer assays.

Another way to probe whether LRRC8-associating proteins contribute to pore properties is to determine whether mutations alter relative permeability. Mutating the homologous T44 residue in LRRC8C, LRRC8D, and LRRC8E to a cysteine increased the relative permeability of I^- compared to Cl^-, in a manner similar to that observed with SWELL1 (Qiu et al., 2014). Interestingly, WT LRRC8D subunits had significantly lower I^- versus Cl^- permeability than either LRRC8C or LRR8CE. These results indicate that not only SWELL1 but also each LRRC8 protein contributes to the permeation properties of VRAC.

The heterogeneity of functional VRAC properties that we observed in bilayers must be a consequence of the diversity of heteromeric channels identified in our biochemical studies. The combination of specific LRRC8 homologs determines intrinsic channel properties, such as conductance and relative permeability. We propose that the heterogeneity of most, if not all, VRAC biophysical properties between different native tissues is regulated by differential expression of LRRC8 isoforms. Interestingly, another common characteristic of VRAC whole-cell current (i.e., its variable inactivation kinetics at high positive potentials) was also shown to depend on LRRC8 homolog composition (Voss et al., 2014). Recently, LRRC8D, but not LRRC8C or LRRC8E, was shown to be required for the influx of certain chemotherapeutics (Planells-Cases et al., 2015). The physiological relevance of having molecularly diverse VRAC channels is currently unknown, but it is likely that cell- and tissue-specific expression of particular LRRC8 proteins is important in specifying roles of VRAC in that tissue. LRRC8C has been reported to contribute to adipocyte differentiation and diet-induced obesity (Hayashi et al., 2011; Tominaga et al., 2004), but whether this is due to its VRAC function is not known. Our results provide the basis to explore these questions through expression analysis and genetic studies of all LRRC8 isoforms.

Volume-Sensing Mechanism of LRRC8 Channel Proteins

How expansion of cell volume is detected and subsequently transduced to VRAC activation is poorly understood. We have taken a minimalistic bilayer approach to study VRAC activation in the absence of cellular components that have been proposed to be involved in this process, such as cytoskeleton, caveoli, enzymes, and second-messenger systems. What we are left with is purified SWELL1-containing LRRC8 complexes and a simple lipid bilayer at the interface between two droplets, which can be experimentally manipulated. We can specifically test effects of mechanically induced stresses on the membrane or a decrease in "intracellular" Γ resulting from diffusion of water across the membrane. Purified complexes in these bilayers are silent, unless an osmotic gradient is imposed between droplets. Under these conditions, we found that injection of isotonic solution into one droplet to increase its volume and perturb the bilayer was not sufficient to induce channel activity, although control experiments indicated that the method activates MscS channels. On the other hand, when bilayers are formed with lower Γ in the *cis* (i.e., cytoplasmic side) droplet, channels were active. Thus, these purified ion channels gate when the ionic concentration is reduced, indicating that SWELL1-containing complexes encode a sensor for low Γ. This intriguing hypothesis that decreased Γ, rather than cell swelling itself, is an adequate stimulus for VRAC was initially proposed by Nilius (Nilius et al., 1998; Sabirov et al., 2000), Strange (Cannon et al., 1998), and their colleagues.

A bacterial transporter OpuA is also triggered directly by a Γ mechanism (Mahmood et al., 2006). In this case, high Γ causes the dissociation of surface-exposed cationic regions from negative phospholipid head groups (electrostatic switching mechanism), leading to conformational changes in the protein (Biemans-Oldehinkel et al., 2006; Poolman et al., 2004). A similar interaction of cationic residues and negatively charged lipids has been described for the mammalian mechanoactivated TREK-1 potassium channel (Chemin et al., 2005). Normal or high Γ may maintain VRAC in a closed conformation so that influx of water and reduction of ionic concentrations gates the channel. For instance, surface-exposed cationic domains, highly charged domains, and salt bridges have been shown to be critical for HCN2 and CNGA1 channel gating (Craven and Zagotta, 2004). The obligatory subunit SWELL1 may encode the sensor, or the sensor may be encoded by each associating subunit or the interfaces they make with SWELL1 or each other. The importance of subunit interfaces to gating is underscored in the ligand-gated ionotropic receptors (Green and Nayeem, 2015). Future mutagenesis and chimeric approaches will enable the identification of the Γ sensor(s) within SWELL1-containing complexes. Predicted cytosolic domains that might be involved in sensing low Γ include the highly cationic TM2-TM3 intracellular loop and proximal C-terminal tail, as well as negatively charged regions in the case of intramolecular interactions. It should be noted, however, that the present study does not address whether low Γ is the only mechanism to activate $I_{Cl,swell}$ in cells; it is likely that other mechanisms play concerted roles. Indeed, it is known that VRAC can also be activated in the absence of cell swelling (Hoffmann et al., 2009).

In summary, we demonstrate that purified SWELL1-containing complexes with at least one other LRRC8 subunit can form functional ion channels that can be directly activated by physiological stimuli. We show, in both minimalistic bilayer systems and HeLa cells, that the particular LRRC8 subunit (LRRC8C-E) associating with SWELL1 determines the single-channel conductance and the relative permeability of $I_{Cl,swell}$ for iodide and chloride, indicating that these family members contribute to the pore. While other pathways such as phosphorylation and cytoskeletal interactions may contribute in intact cells, a sensor for low Γ is an integral part of purified SWELL1-containing complexes. With these new data, the structural requirements for VRAC activation may now be addressed. A more complete understanding of volume-sensing mechanisms will undoubtedly lead to insights into the physiological roles of VRAC and help guide future therapeutic approaches in ischemia, stroke, and other pathologies.

EXPERIMENTAL PROCEDURES

Electrophysiology

Whole-cell patch-clamp recordings were performed as described previously (Qiu et al., 2014), except, in permeability studies, recording pipettes contained (in millimolar): 130 CsCl, 10 HEPES, 4 MgATP (pH 7.2); LRRC8(B/C/D/E)$^{-/-}$ HeLa Flp-In T-REx cells were transfected with WT or T44C LRRC8C, LRRC8D, or LRRC8E and cultured without TET; and the experimenter was blinded to cell type. Cell-attached patch recordings were made on swollen cells using 7- to 15-MΩ pipettes containing (in millimolar): 95 N-methyl-D-glucamine (NMDG), 4 $MgCl_2$, 4 NaCl, 5 TEA-Cl, 10 HEPES, 5 dextrose, 0.1 $CdCl_2$, and 100 mannitol, using a protocol modified from previous studies (Okada et al., 1994; Wang et al., 2005). Cells were bathed in a high extracellular KCl solution (either 265 or 300 mOsm) to depolarize cells toward 0 mV and to inhibit RVD (Okada et al., 1994). The 265-mOsm solution contained (in millimolar): 100 KCl, 1.5 $CaCl_2$, 1 $MgCl_2$, 10 HEPES, 10 dextrose, KOH to pH 7.4, and 265 mOsm/kg with mannitol (Vapro Vapor Pressure Osmometer, Wescor). The 300 mOsm solution included extra mannitol (35 mM).

Reconstitution of SWELL1-Containing Complexes in Droplet Lipid Bilayers

Droplet lipid bilayers were formed as described previously (Bayley et al., 2008; Syeda et al., 2008). Briefly, lipid bilayers were formed between two droplets containing (in millimolar): 0.5 1,2-diphytanoyl-sn-glycero-3-phosphocholine (DPhPC), 500 KCl, 20 HEPES, at pH 7.4 in a hexadecane medium. For low Γ experiments, 500 mM KCl was replaced by either 150 or 70 mM KCl. Protein was added in the form of proteoliposomes in the *cis* droplet. Only single-channel records were selected for analysis to avoid anomalies in conductance and open probability determination; however, multiple channels were also observed.

Isotonic and Hypotonic Conditions in Droplet Lipid Bilayers

Mannitol (300 mM) was supplemented asymmetrically in the *cis* droplet to generate an osmolality imbalance, causing water flux into the *cis* droplet. An isotonic condition refers to the symmetric solution in both droplets (e.g., 500, 150, or 70 mM KCl, or 70 mM KCl + 160 mM mannitol).

Protein Orientation in Droplet Lipid Bilayers

We used the ATP-sided block approach as previously described for whole-cell VRAC currents (Jackson and Strange, 1995) to block inserted channels in the outside-in configuration. In this method, the *cis* droplet contained Na_2-ATP (4 mM). Activated SWELL1-containing complexes were blocked by adding 4 mM Na_2-ATP to the *trans* droplet, indicating extracellular domains faced the *trans* droplet. Channels usually inserted so that the intracellular side of the protein remained in the *cis* droplet.

SUPPLEMENTAL INFORMATION

Supplemental Information includes Supplemental Experimental Procedures, six figures, and four tables and can be found with this article online at http://dx.doi.org/10.1016/j.cell.2015.12.031.

AUTHOR CONTRIBUTIONS

R.S. designed, performed, and analyzed the experiments related to reconstitution of protein in lipid bilayers. Z.Q. initiated and led the study and performed all aspects of biochemistry with help from M.N.F. Z.Q., M.N.F., and S.M.C. generated knockout cell lines. A.E.D. co-initiated the study, contributed to research strategy, and conducted whole-cell and cell-attached patch experiments. S.E.M. performed and analyzed single-channel experiments in cells. D.E.M. and E.C.P. performed mass spectrometry analysis, J.M. provided molecular cloning support, and M.M. provided lab resources and critical insight into the manuscript. R.S., Z.Q., A.E.D., and A.P. wrote the manuscript.

ACKNOWLEDGMENTS

We thank Jose Santos for helpful discussions on biochemistry and protein reconstitution; Shuying Sun for help in generating stable Flp-In cell lines; and Michael Bandell, David Jones, and Jie Xu for technical assistance in biochemistry. R.S. thanks Syed Asleh Al-Husaini for encouragement and support. This work was partly supported by grants from NIH awarded to A.P. (NS083174) and M.M. (GM49711). A.P. is an Investigator of the Howard Hughes Medical Institute.

Received: November 2, 2015
Revised: November 16, 2015
Accepted: December 4, 2015
Published: January 28, 2016

REFERENCES

Abascal, F., and Zardoya, R. (2012). LRRC8 proteins share a common ancestor with pannexins, and may form hexameric channels involved in cell-cell communication. BioEssays *34*, 551–560.

Akita, T., and Okada, Y. (2014). Characteristics and roles of the volume-sensitive outwardly rectifying (VSOR) anion channel in the central nervous system. Neuroscience *275*, 211–231.

Anishkin, A., Loukin, S.H., Teng, J., and Kung, C. (2014). Feeling the hidden mechanical forces in lipid bilayer is an original sense. Proc. Natl. Acad. Sci. USA *111*, 7898–7905.

Battle, A.R., Petrov, E., Pal, P., and Martinac, B. (2009). Rapid and improved reconstitution of bacterial mechanosensitive ion channel proteins MscS and MscL into liposomes using a modified sucrose method. FEBS Lett. *583*, 407–412.

Bayley, H., Cronin, B., Heron, A., Holden, M.A., Hwang, W.L., Syeda, R., Thompson, J., and Wallace, M. (2008). Droplet interface bilayers. Mol. Biosyst. *4*, 1191–1208.

Biemans-Oldehinkel, E., Mahmood, N.A., and Poolman, B. (2006). A sensor for intracellular ionic strength. Proc. Natl. Acad. Sci. USA *103*, 10624–10629.

Brohawn, S.G., Su, Z., and MacKinnon, R. (2014). Mechanosensitivity is mediated directly by the lipid membrane in TRAAK and TREK1 K^+ channels. Proc. Natl. Acad. Sci. USA *111*, 3614–3619.

Cannon, C.L., Basavappa, S., and Strange, K. (1998). Intracellular ionic strength regulates the volume sensitivity of a swelling-activated anion channel. Am. J. Physiol. *275*, C416–C422.

Chemin, J., Patel, A.J., Duprat, F., Lauritzen, I., Lazdunski, M., and Honoré, E. (2005). A phospholipid sensor controls mechanogating of the K+ channel TREK-1. EMBO J. *24*, 44–53.

Craven, K.B., and Zagotta, W.N. (2004). Salt bridges and gating in the COOH-terminal region of HCN2 and CNGA1 channels. J. Gen. Physiol. *124*, 663–677.

Green, T., and Nayeem, N. (2015). The multifaceted subunit interfaces of ionotropic glutamate receptors. J. Physiol. *593*, 73–81.

Hayashi, T., Nozaki, Y., Nishizuka, M., Ikawa, M., Osada, S., and Imagawa, M. (2011). Factor for adipocyte differentiation 158 gene disruption prevents the body weight gain and insulin resistance induced by a high-fat diet. Biol. Pharm. Bull. *34*, 1257–1263.

Hille, B. (2001). Ion Channels of Excitable Membranes (Sunderland, MA: Sinauer Associates, Inc.).

Hoffmann, E.K., Lambert, I.H., and Pedersen, S.F. (2009). Physiology of cell volume regulation in vertebrates. Physiol. Rev. *89*, 193–277.

Jackson, P.S., and Strange, K. (1995). Characterization of the voltage-dependent properties of a volume-sensitive anion conductance. J. Gen. Physiol. *105*, 661–676.

Kubota, K., Kim, J.Y., Sawada, A., Tokimasa, S., Fujisaki, H., Matsuda-Hashii, Y., Ozono, K., and Hara, J. (2004). LRRC8 involved in B cell development belongs to a novel family of leucine-rich repeat proteins. FEBS Lett. *564*, 147–152.

Kunzelmann, K. (2015). TMEM16, LRRC8A, bestrophin: chloride channels controlled by Ca(2+) and cell volume. Trends Biochem. Sci. *40*, 535–543.

Lee, C.C., Freinkman, E., Sabatini, D.M., and Ploegh, H.L. (2014). The protein synthesis inhibitor blasticidin s enters mammalian cells via leucine-rich repeat-containing protein 8D. J. Biol. Chem. *289*, 17124–17131.

Mahmood, N.A.B.N., Biemans-Oldehinkel, E., Patzlaff, J.S., Schuurman-Wolters, G.K., and Poolman, B. (2006). Ion specificity and ionic strength dependence of the osmoregulatory ABC transporter OpuA. J. Biol. Chem. *281*, 29830–29839.

Nilius, B., Eggermont, J., Voets, T., and Droogmans, G. (1996). Volume-activated Cl- channels. Gen. Pharmacol. *27*, 1131–1140.

Nilius, B., Prenen, J., Voets, T., Eggermont, J., and Droogmans, G. (1998). Activation of volume-regulated chloride currents by reduction of intracellular ionic strength in bovine endothelial cells. J. Physiol. *506* (Pt. 2), 353–361.

Okada, Y. (1997). Volume expansion-sensing outward-rectifier Cl- channel: fresh start to the molecular identity and volume sensor. Am. J. Physiol. *273*, C755–C789.

Okada, Y., Petersen, C.C., Kubo, M., Morishima, S., and Tominaga, M. (1994). Osmotic swelling activates intermediate-conductance Cl- channels in human intestinal epithelial cells. Jpn. J. Physiol. *44*, 403–409.

Pedersen, S.F., Klausen, T.K., and Nilius, B. (2015). The identification of a volume-regulated anion channel: an amazing Odyssey. Acta Physiol. (Oxf.) *213*, 868–881.

Planells-Cases, R., Lutter, D., Guyader, C., Gerhards, N.M., Ullrich, F., Elger, D.A., Kucukosmanoglu, A., Xu, G., Voss, F.K., Reincke, S.M., et al. (2015). Subunit composition of VRAC channels determines substrate specificity and cellular resistance to Pt-based anti-cancer drugs. EMBO J. *34*, 2993–3008.

Poolman, B., Spitzer, J.J., and Wood, J.M. (2004). Bacterial osmosensing: roles of membrane structure and electrostatics in lipid–protein and protein–protein interactions. Biochim. Biophys. Acta *1666*, 88–104.

Qiu, Z., Dubin, A.E., Mathur, J., Tu, B., Reddy, K., Miraglia, L.J., Reinhardt, J., Orth, A.P., and Patapoutian, A. (2014). SWELL1, a plasma membrane protein, is an essential component of volume-regulated anion channel. Cell *157*, 447–458.

Sabirov, R.Z., Prenen, J., Tomita, T., Droogmans, G., and Nilius, B. (2000). Reduction of ionic strength activates single volume-regulated anion channels (VRAC) in endothelial cells. Pflugers Arch. *439*, 315–320.

Solc, C., and Wine, J. (1991). Swelling-induced and depolarization-induced Cl^- channels in normal and cystic fibrosis epithelial cells. Am. J. Physiol. *261*, C658–C674.

Syeda, R., Holden, M.A., Hwang, W.L., and Bayley, H. (2008). Screening blockers against a potassium channel with a droplet interface bilayer array. J. Am. Chem. Soc. *130*, 15543–15548.

Tominaga, K., Kondo, C., Kagata, T., Hishida, T., Nishizuka, M., and Imagawa, M. (2004). The novel gene fad158, having a transmembrane domain and

leucine-rich repeat, stimulates adipocyte differentiation. J. Biol. Chem. *279*, 34840–34848.

Trouet, D., Nilius, B., Jacobs, A., Remacle, C., Droogmans, G., and Eggermont, J. (1999). Caveolin-1 modulates the activity of the volume-regulated chloride channel. J. Physiol. *520*, 113–119.

Tsumura, T., Oiki, S., Ueda, S., Okuma, M., and Okada, Y. (1996). Sensitivity of volume-sensitive Cl- conductance in human epithelial cells to extracellular nucleotides. Am. J. Physiol. *271*, C1872–C1878.

Voss, F.K., Ullrich, F., Münch, J., Lazarow, K., Lutter, D., Mah, N., Andrade-Navarro, M.A., von Kries, J.P., Stauber, T., and Jentsch, T.J. (2014). Identification of LRRC8 heteromers as an essential component of the volume-regulated anion channel VRAC. Science *344*, 634–638.

Wang, J., Xu, H., Morishima, S., Tanabe, S., Jishage, K., Uchida, S., Sasaki, S., Okada, Y., and Shimizu, T. (2005). Single-channel properties of volume-sensitive Cl- channel in ClC-3-deficient cardiomyocytes. Jpn. J. Physiol. *55*, 379–383.

Weiss, H., and Lang, F. (1992). Ion channels activated by swelling of Madin Darby canine kidney (MDCK) cells. J. Membr. Biol. *126*, 109–114.

Wittig, I., Beckhaus, T., Wumaier, Z., Karas, M., and Schägger, H. (2010). Mass estimation of native proteins by blue native electrophoresis: principles and practical hints. Mol. Cell. Proteomics *9*, 2149–2161.

Zhou, H.-X., Rivas, G., and Minton, A.P. (2008). Macromolecular crowding and confinement: biochemical, biophysical, and potential physiological consequences. Annu. Rev. Biophys. *37*, 375–397.

Cell

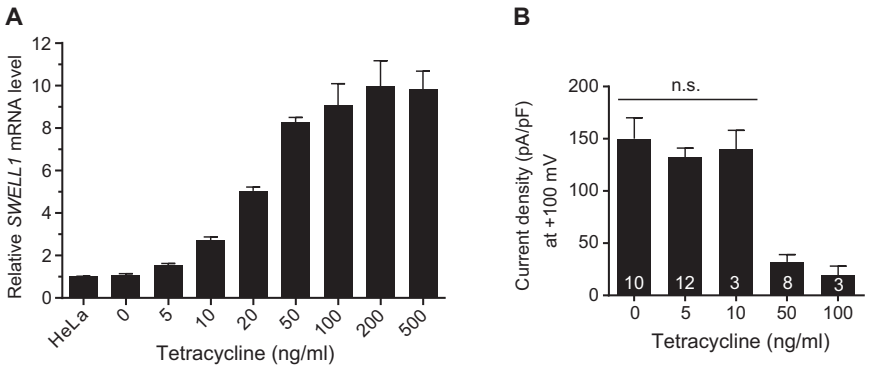

Figure S1. Characterization of a Stable HeLa Cell Line Expressing SWELL1-FLAG Using an Inducible Flp-In System, Related to Figure 1

(A) *SWELL1* mRNA expression level in tetracycline-induced HeLa cells was assayed by qPCR and normalized to the endogenous *SWELL1* level in WT HeLa cells. Error bars indicate SEM (n = 2).

(B) Whole cell current densities (at +100 mV) of maximally activated $I_{Cl,swell}$ in tetracycline-induced HeLa cells. Number of cells tested is shown inside the bars.

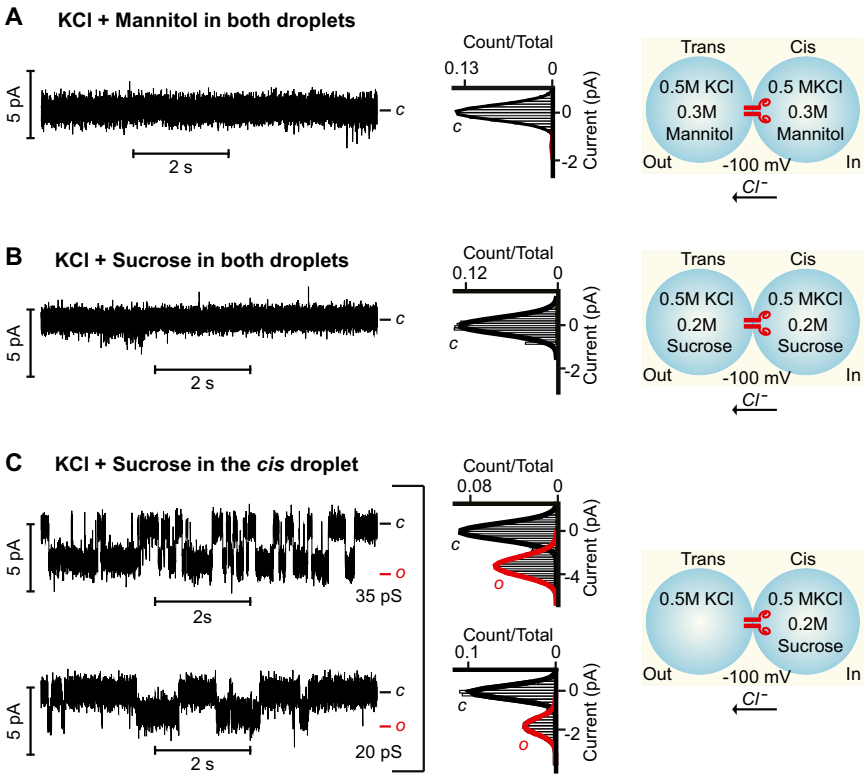

Figure S2. SWELL1-Containing Complex Reconstituted in Droplet Lipid Bilayers under Symmetric Osmolyte Conditions or When Challenged with a Sucrose Gradient, Related to Figure 1

(A) A representative trace of the current recordings (n = 10) and the corresponding all-point histogram of SWELL1-containing complexes under isotonic conditions and symmetrical 300 mM mannitol across the lipid bilayer. All-points histogram of the data shown on the right indicate closed state *(c)*. Illustration of experimental setup and conditions used to reconstitute channels in lipid bilayers are indicated in the right panel.

(B) Current recordings and the corresponding all-point current histogram of SWELL1-containing complexes under isotonic conditions and symmetric 200 mM sucrose (n = 7). Experimental conditions are illustrated in the right panel.

(C) Single-channel currents and corresponding all-point histograms of SWELL1-containing complexes under hypotonic conditions generated by a 200 mM sucrose gradient across the lipid bilayers (n = 11). *Cis* droplet is connected to the active electrode and *trans* droplet is connected to the grounded electrode, such that at negative applied potentials anions move from *cis* to *trans* (shown by an arrow), thus downward current deflections.

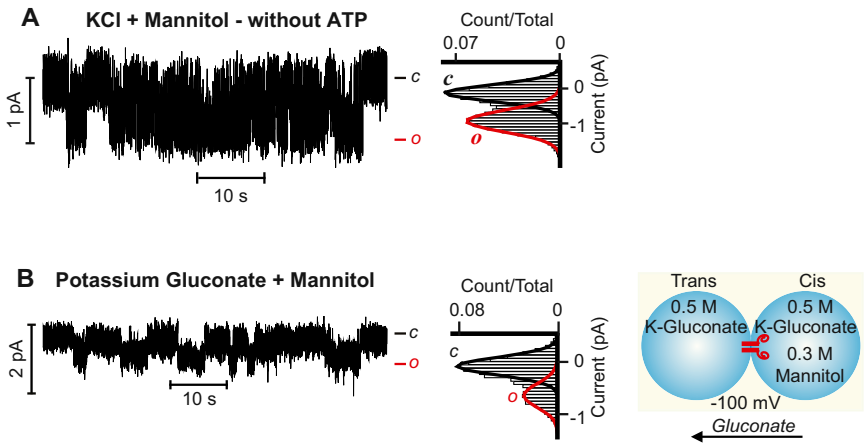

Figure S3. SWELL1-Containing Complex Reconstituted in Droplet Lipid Bilayer in Various Conditions, Related to Figure 1

(A) Single-channel current recordings in 500 mM KCl and the corresponding all-point histogram of SWELL1-containing complexes under hypotonic conditions generated by a 300 mM mannitol gradient as shown in Figure 1. In this experiment, both droplets lack Na_2-ATP. All-points histogram of the data shown on the right indicates closed state *(c)* and open state *(o)* of the channel (n = 5).

(B) SWELL1-containing complex reconstituted in droplet lipid bilayers with K-Gluconate replacing KCl. Single-channel currents and the corresponding all-point current histogram under hypotonic conditions generated by a 300 mM mannitol gradient across the lipid bilayers (left panel). All-points histogram of the data (n = 6) indicate closed (*c)* and open (*o)* states. Experimental conditions are illustrated in the right panel.

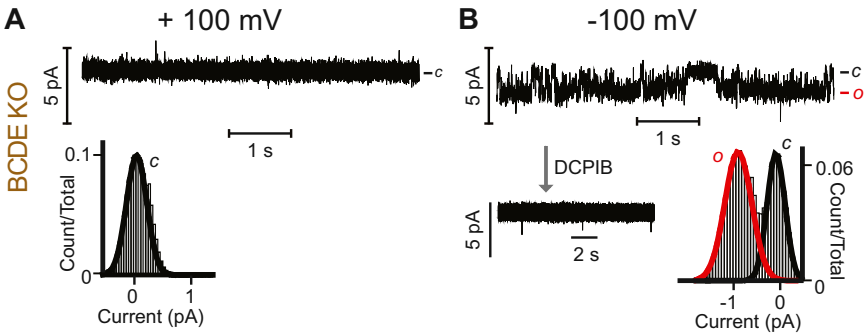

Figure S4. SWELL1 Proteins Purified from *LRRC8(B/C/D/E)*$^{-/-}$ Cells Reconstituted in Droplet Lipid Bilayers, Related to Figure 2

(A-B) Single-channel recordings under hypotonic conditions and corresponding all-point current histograms of SWELL1 complexes purified from the *LRRC8*(B/C/D/E)$^{-/-}$ cells, (A) at +100 mV and (B) at −100 mV (n = 6). The inset below the record shows block after injecting 40 μM DCPIB (final) into the *cis* droplet. *c* and *o* indicate closed and open states, respectively.

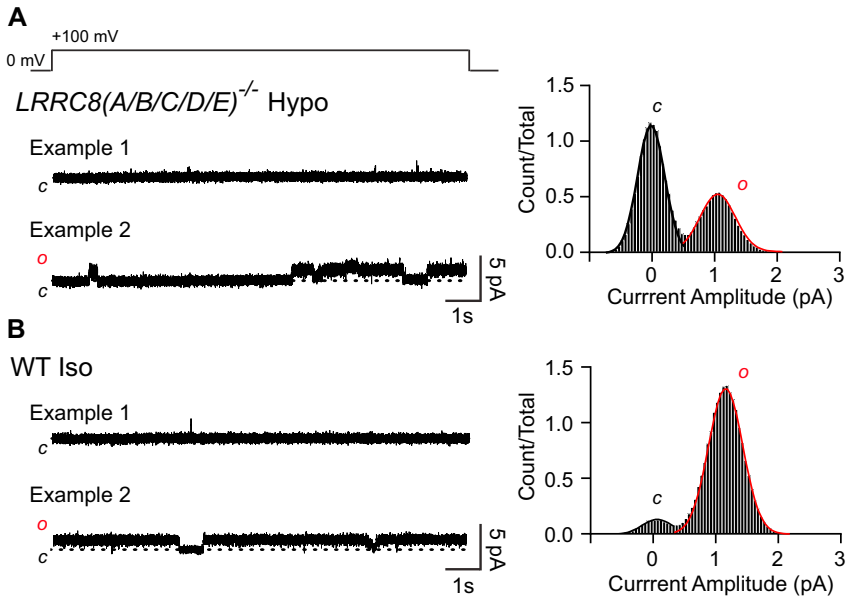

Figure S5. Background Currents Observed in WT and *LRRC8 (A/B/C/D/E)*$^{-/-}$ HeLa cells, Related to Figure 3

(A) ABCDE KO HeLa cells in 265 mOsm/Kg hypotonic solution. Left: representative 10 s long trace from two separate cells showing a silent patch (Example 1) and a patch with background single-channel activity (Example 2). The voltage step is indicated above the trace. Right: All-points histogram of trace in Example 2 indicating single-channel amplitude of the background channel (1.04 pA). Pipette potential, −100 mV.

(B) WT HeLa cells in 300 mOsm/Kg isotonic solution. Left: representative 10 s long current trace from two separate cells showing a silent patch (Example 1) and a patch with single-channel activity (Example 2). Right: All-points histogram of trace in Example 2 indicating single-channel amplitude of the background channel (1.15 pA). Pipette potential, −100 mV.

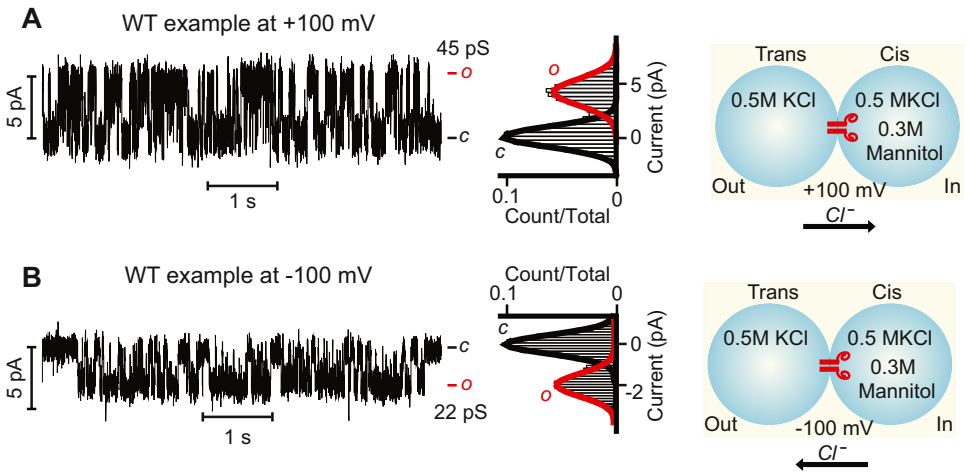

Figure S6. SWELL1-Containing Complexes Purified from WT HeLa Cells Exhibit Single-Channel Rectification in Lipid Bilayers, Related to Figure 4

(A) An example of single-channel recording performed at +100 mV in the presence of symmetric 500 mM KCl and osmotic gradient generated by 300 mM mannitol in the *cis* droplet.

(B) The example of a single-channel recording (continuation from panel A) at −100 mV under similar experimental conditions as described for (A). The channel exhibits higher conductance at positive potentials as compared to negative (n > 30).

Cell

Supplemental Information

LRRC8 Proteins Form Volume-Regulated Anion Channels that Sense Ionic Strength

Ruhma Syeda, Zhaozhu Qiu, Adrienne E. Dubin, Swetha E. Murthy, Maria N. Florendo, Daniel E. Mason, Jayanti Mathur, Stuart M. Cahalan, Eric C. Peters, Mauricio Montal, and Ardem Patapoutian

Supplemental Experimental Procedures.

Cell culture and generation of an inducible cell line. A stable HeLa cell line expressing a tetracycline-inducible FLAG-tagged SWELL1 was created based on the Flp-In T-REx System (Life Technologies) according to the manufacturer's manual. In brief, a single Flp recognition target (FRT) site was stably integrated in the HeLa cell genome (Flp-In HeLa). Human SWELL1 coding sequence was PCR amplified with a carboxy-terminal FLAG tag (DYKDDDDK), sub-cloned into pcDNA5/FRT/TO using KpnI and EcoRV restriction enzyme sites, and then co-transfected into Flp-In HeLa cells along with a plasmid expressing the FLP recombinase (pOG44, Life technologies). After selection in 200 μg ml^{-1} hygromycin, single colonies were picked and expanded. Stable HeLa cells were grown in Dulbecco's Modified Eagle Medium (DMEM) containing 4.5 mg ml^{-1} glucose, 10% tetracycline-free fetal bovine serum (Clontech) and penicillin/streptomycin. For electrophysiological experiments, cells were seeded on 12 mm diameter poly-D-lysine coated glass coverslips (BD) in 24 well dishes and transfected using Lipofectamine 2000 (Life Technologies) according to the manufacturer's instruction. 500 ng ml^{-1} of plasmid DNA together with 250 ng ml^{-1} GFP plasmid were co-transfected and cells were recorded 18-48 h later.

Generation of knockout cell lines. To disrupt *LRRC8* genes in SWELL1 inducible HeLa cells, we utilized CRISPR/Cas9-mediated gene deletion (Ran et al., 2013). The targeting guide RNA sequences used for all genes were as previously reported (Voss et al., 2014) except for the LRRC8C-targeting sequence (3C: 5'-GTTATGAGCGAGCCCTCCAC-3', positive strand). Guide RNAs were cloned into PX458-mCherry, a modification of the plasmid pSpCas9(BB)-2A-GFP (PX458), which was a gift from Feng Zhang (Addgene plasmid # 48138) (Ran et al., 2013). To disrupt multiple *LRRC8* genes simultaneously, multiple plasmids were transfected together into HeLa cells using Lipofectamine 2000 (Life Technologies). Two to three days post-transfection single fluorescent cells were FACS-sorted into 96-well plates containing DMEM with 20% FBS. Single colonies were isolated and expanded for genotyping analysis of frameshift mutations by target-site-specific PCR and TA cloning followed by Sanger-sequencing (**Tables S3**). The absence of LRRC8 proteins in the purified samples from selective HeLa inducible cell clones was also confirmed by label-free mass spectrometry quantification (**Figure 2B**). For WT HeLa cells, before disrupting *LRRC8* genes, a FLAG tag was first inserted at the C-terminus of SWELL1 with CRISPR/Cas9 technology as described (Ran et al., 2013) co-transfecting a 200 bp single-stranded DNA oligo and PX458 carrying SWELL1-targeting sequence (5'-GTGCTGGGCCGGCCTCGCTC-3', negative strand). Clones in which SWELL1 was not inadvertently mutated (other than the insertion of FLAG tag) were selected based on target-site-specific PCR and TA cloning followed by Sanger-sequencing (**Tables S4**).

Quantitative real-time PCR. To induce SWELL1-FLAG expression, cells were treated with 0 to 500 ng ml^{-1} tetracycline for 24 h. Total RNA were then isolated using TRIzol reagent (Life Technologies) and were used to generate the 1st strand cDNA using the QuantiTect Reverse Transcription kit (QIAGEN). Taqman qPCR assays for human *SWELL1* (assay id: Hs.PT.49a.14499917) and human *GAPDH* (assay id: Hs.PT.39a.22214836) were obtained from IDT. The reaction was run in the ABI 7900HT fast real time system using 0.5 μl of the cDNA in a 10 μl reaction with FastStart Universal probe master mix (Roche) according to the manufacturer's instruction in triplicate. *GAPDH* was used as the reference gene. Calibrations and normalizations were done using the $2^{-\Delta\Delta CT}$ method.

Protein purification and NativePAGE Novex Bis-Tris gel. WT HeLa cells or HeLa cells expressing SWELL1-FLAG using an inducible Flp-In T-REx system (treated with 0 or 5 ng ml^{-1} tetracycline for 24 h) were collected and homogenized in a hypotonic buffer containing 20 mM Tris (pH 7.5), 50 mM NaCl and a cocktail of protease inhibitors with a dounce homogenizer. The cell lysate was centrifuged at 2,000 x *g* for 10 min at 4°C. The supernatant was collected and centrifuged at 167,000 x *g* for 45 min at 4°C. The resulting membrane pellet was rinsed in the washing buffer containing 20 mM Tris (pH 7.5), 150 mM NaCl and a cocktail of protease inhibitors and lysed in the washing buffer with 1% (w/v) n-Dodecyl-β-maltoside (DDM). Dynabeads Protein G (Life Technologies) were bound with M2 anti-FLAG antibody (F3165, Sigma) according to the manufacturer's instruction, and then incubated with the lysates at 4°C overnight. The beads were washed five times and eluted with 50 μg ml^{-1} 3X FLAG peptide (Sigma) in a buffer containing 20 mM Tris (pH7.5), 150 mM NaCl, 0.05% DDM and a cocktail of protease inhibitors. The purified samples were mixed with NativePAGE Sample Buffer and NativePAGE 5% G-250 Sample Additive and then subjected to 4-16% NativePAGE Novex Bis-Tris gel for electrophoresis at 150 V for 2 h according to the manufacturer's instruction (Life technologies). After electrophoresis, the native gel was then either visualized by the fast Coomassie G-250 staining system (GenScript) or transferred to a PVDF membrane for western blotting.

Western blotting. After electrophoresis, native and denaturing PAGE gels were transferred to PVDF membranes. Transferred membranes were then blocked with 5% milk in TBS buffer with 0.1% Tween-20 at room temperature for

1 h, incubated with anti-SWELL1 antibody (1:400; HPA016811, Sigma) at 4°C overnight and followed by peroxidase-conjugated anti-rabbit IgG secondary antibody (1:10,000) at room temperature for 1 h. Proteins were detected with SuperSignal West Femto Substrate (Thermo Scientific).

Paraformaldehyde and formaldehyde crosslinking. Live cells were washed in PBS, resuspended in 1% paraformaldehyde (PFA) at room temperature for 8 min, and followed by adding 125 mM glycine to stop the PFA crosslinking reaction. Treated cells were collected and subjected to subsequent steps of protein purification, 4-16% NativePAGE Novex Bis-Tris gel for native electrophoresis, and western blotting with the anti-FLAG antibody. For formaldehyde (FA) crosslinking, the purified samples were treated with or without 0.3% FA at room temperature and then mixed with NuPAGE LDS Sample Buffer at indicated time points, followed by heating at 70°C for 10 min to denature the protein. The samples were then subjected to 3-8% NuPAGE Tris-Acetate gel (Life technologies) electrophoresis under denaturing conditions.

Mass spectrometry. Purified samples were separated on 4-16% NativePAGE Novex Bis-Tris gel and visualized by fast Coomassie G-250 staining. The gel band containing the SWELL1 complex or the corresponding blank band from the control sample above the 720 kDa protein marker was excised and subjected to mass spectrometry. In brief, gel bands were de-stained, reduced with DTT, alkylated with iodoacetamide, digested with trypsin overnight and dried *in vacuo* (Shevchenko et al., 1996). Dried samples were reconstituted in 40 μL 0.1% formic acid and analyzed for absolute quantitation on a Sciex QTRAP 6500 or label free quantitation on a Q-Exactive.

For absolute quantitation of LRRC8 proteins, MRM transitions were prepared and optimized for the tryptic peptides from the five LRRC8 proteins using Skyline 2.1. The most intense peptide from each protein and the three most intense transitions were selected for the MRM analysis (**Table S2**). Stable isotope labeled peptides were synthesized at >95% purity (Thermo Scientific) and spiked into digests for absolute quantitation. For analysis, 10 μL of reconstituted sample was mixed with an equal volume of standard peptide solution, 22.22 nM (high), 2.47 nM (medium), or 0.27 nM (low). A separate eight point standard curve of standard peptides was prepared from 200 nM to 0.09 nM. Samples were loaded on a 360x100 μm precolumn (Kasil frit, 2 cm Monitor C18) prior to separation on a 360x75 μm (15 cm Monitor C18) integrated column/emitter packed in house and using a Nanospray III source. After loading, peptides were separated with a linear gradient from 2 to 40% B (B: 0.1% formic acid, 90% ACN; 500 nL/min) in 9 min. The QTRAP 6500 was operated in unit resolution for Q1 and Q3 with the following parameters: Cur Gas 30, IS at 2500V, GS1 at 20, IHT at 190, CAD at medium, EP at 10V and CXP at 13V. Transitions were scheduled with a 120 s window and target of 0.5 s. The data was analyzed in MultiQuant 2.1 by summing the peak areas from all transitions and using a weighting of 1/x for the standard curve. The standard curve was then applied to the "unknown" samples with defined amounts of spiked internal standard. Typically, all three spiked concentrations were averaged to determine the concentration of the protein.

For label-free quantitation of LRRC8 proteins, samples were analyzed on a column setup similar to that described above with a linear gradient from 2 to 35% B (B: 0.1% formic acid, ACN; 500 nL/min) in 60 min using Q-Exactive parameters denoted as "sensitive" by Kelstrup and colleagues (Kelstrup et al., 2012). The data were analyzed for label-free relative quantitation using Progenesis QI for Proteomics (Nonlinear Dynamics). Here the data files were imported and automatically aligned. Peaks were chosen with charges from 2-6 and the default normalization accepted. Peptide identification was performed using Mascot against a human slice of the UniProt database downloaded in May 2012, and search results were filtered for an expect cut off of 0.01. The relative quantitation was focused on the LRRC8 proteins using non-conflicting peptides.

Molecular biology. Human LRRC8D cDNA in pCMV6-AC was obtained from OriGene. Human LRRC8C and LRRC8E open reading frames in pCMV6-Entry were obtained from OriGene and then PCR amplified and sub-cloned into pIRES2-EGFP (Clontech) using NheI/BamHI and XhoI/EcoRI restriction enzyme sites, respectively. Cysteine mutations were introduced into these constructs using QuikChange II XL site-directed mutagenesis kit (Agilent Technologies) following the manufacturer's instruction.

Formation of Proteoliposomes. Proteoliposomes were formed by incorporating purified protein in asolectin liposomes. First, asolectin liposomes (5 mg/mL) were prepared by resuspending dried asolectin lipids (L-α-phosphatidylcholine, Avanti Polar lipids Cat # 840054) in 200 mM KCl, 10 mM HEPES, pH 7.2. The liposomes were then extruded through a 0.1 mm filter (Whatman Nuclepore Track-Etch membrane). Asolectin liposomes (400 μL at 5 mg/mL) were semi-permeabilized for 1 h at room temperature with rotation, by adding 18 μL DDM (200 mM stock). Purified SWELL1-containing complex (5-10 μL) was added in semi-permeabilized liposomes and incubated with rotation at room temperature for 1 h. This sample was then subjected to Slide-A-Lyzer dialysis cassette with molecular

cut off weight 3.5 kDa (Thermo Scientific, Prod. # 66330) to eliminate excess detergent and FLAG peptide which has a molecular weight of 1.0 kDa for FLAG and 2.8 kDa for 3xFLAG peptide. The dialysis was performed at 4 ºC against 500 mL of 200 mM KCl, 10 mM HEPES, pH 7.2. The dialysis buffer was replaced in full after 6 h and again after 12 h. The dialysed sample was ultracentrifuged in a TLA rotor to pellet the proteoliposomes at 60,000 x g for 1 h at 12 ºC. The detergent free proteoliposomes were resuspended in 40 μL of buffered solution (200 mM KCl, 10 mM HEPES, pH 7.4). The proteoliposomes sample served as the starting material for subsequent protein reconstitution in droplet lipid bilayers.

Cell-attached patch recordings. The cells used for cell-attached patch studies were WT HeLa cells engineered to express endogenous SWELL1 containing a C-terminal FLAG tag and these cells with LRRC8 genes knocked out using CRISPR (*LRRC8(B/D/E)*$^{-/-}$ and *LRRC8(B/C/E)*$^{-/-}$ expressing endogenous SWELL1-FLAG with either LRRC8C or LRRC8D, respectively, and *LRRC8(A/B/C/D/E)*$^{-/-}$ expressing no $I_{Cl,swell}$). Cells on poly-D-lysine-coated 12 mm glass coverslips at 10-50% confluency were placed into high K^+ solution and 5-20 min later the cell-attached configuration was achieved. Long (10 s) step potentials were applied to +120, +100 and +80 mV from a holding potential of either RP-0 or RP-50 mV (results were similar) followed by a step to negative voltages (-100, -120 mV) in some cases, every 10 or 20 s. In some cases 10 s steps to +100 mV were repeated every 10 s. Single-channel currents from HeLa, *LRRC8(B/D/E)*$^{-/-}$ and *LRRC8(B/C/E)*$^{-/-}$ cells had five VRAC-like characteristics: they were (i) dependent on cell swelling in HYPO 265 (>1.7 pA currents were not observed in any of the non-swollen HeLa cells (n= 10, 12 and 8 for WT, *LRRC8(B/D/E)*$^{-/-}$ and *LRRC8(B/C/E)*$^{-/-}$ cells, respectively)), (ii) rectifying, (iii) inactivating at very positive potentials (+120 mV, data not shown), and (iv) active at negative potentials with few closures (data not shown). When observed, channels would be open at the beginning of the depolarizing voltage step (a hallmark of VRAC) either immediately after sealing or develop within 15 min. Channel activity usually ran down over time in the cell-attached configuration (data not shown). Cell-attached patch recordings from *LRRC8(A/B/C/D/E)*$^{-/-}$ negative control cells revealed only very small (~1 pA) currents that were observed in both ISO and HYPO conditions and were not time-linked to the beginning of the step to positive voltages (**Figure 3A**; n=20 separate cells; **Figure S5**). Single-channel amplitudes were measured by fitting a Gaussian equation to the all-points histograms using Clampfit 10.3 software. In patches where more than one channel was observed, amplitude was calculated as a difference in histogram peaks. Often a single patch would contain channel activity with at least two distinct sizes. Histograms of current amplitudes observed for each patch were plotted and average values were made around modes. Thus, a single value in **Figure 3** represents the size of a single-channel current observed in a single patch. Only one patch was recorded per cell. Single-channel data from *LRRC8(B/C/D)*$^{-/-}$ was attempted but the extremely rare occurrence of closures observed at +100 mV made this channel difficult to study. Frequency distributions of single-channel amplitudes shown in **Figure 3** include only channels with amplitudes greater than 1.7 pA (two standard deviations above the mean background current amplitude).

Data Analysis. All the single-channel recordings conducted in droplet bilayers were acquired at 10 kHz and online-filtered at 2 kHz. Additional offline-filtering of 1 kHz was applied for the purpose of analysis and display. Traces shown in **Figure 1J** and **Figure S4** were additionally filtered at 500 Hz for analysis and display. The single-channel recordings conducted in cells were sampled at 20 kHz (50 μs) and filtered at 2 kHz with a lowpass Bessel filter. Additional 1 kHz offline filtering was applied for data analysis and display. Statistical significance was evaluated using unpaired two-tailed Student's *t*-test for comparing the difference between two samples, and ANOVA for comparing multiple groups. Single-channel conductance (γ) was calculated for each experiment by fitting a Gaussian curve to the all-point current histograms. The current-amplitudes obtained from the histograms were divided by the applied voltage to calculate γ. For **Figure 2D-2H** each calculated conductance was plotted as an individual value. For **Figures 4D-4I** and **6,** conductance is plotted as mean ± S.E.M from the indicated number of experiments (n).

Supplemental References

Kelstrup, C.D., Young, C., Lavallee, R., Nielsen, M.L., and Olsen, J. V. (2012). Optimized fast and sensitive acquisition methods for shotgun proteomics on a quadrupole orbitrap mass spectrometer. J. Proteome Res. *11*, 3487–3497.

Ran, F.A., Hsu, P.P.D., Wright, J., Agarwala, V., Scott, D. A, and Zhang, F. (2013). Genome engineering using the CRISPR-Cas9 system. Nat. Protoc. *8*, 2281–2308.

Shevchenko, A., Wilm, M., Vorm, O. and Mann, M. (1996). Mass spectrometric sequencing of proteins from silver-stained polyacrylamide gels. Anal. Chem. *68*, 850–858.

Table S1: Mass spectrometry of native gel band containing samples purified from control HeLa cells and SWELL1-FLAG expressing cells. Related to figure 1.

Identified Proteins	Number of unique peptides		
	Control	SWELL1 sample #1	SWELL1 sample #2
Leucine-rich repeat-containing protein 8A OS=Homo sapiens GN=LRRC8A/SWELL1	0	39	47
Keratin, type II cytoskeletal 1 OS=Homo sapiens GN=KRT1	20	23	20
Leucine-rich repeat-containing protein 8D OS=Homo sapiens GN=LRRC8D	0	33	34
Leucine-rich repeat-containing protein 8E OS=Homo sapiens GN=LRRC8E	0	26	31
Keratin, type I cytoskeletal 9 OS=Homo sapiens GN=KRT9	8	16	14
Leucine-rich repeat-containing protein 8C OS=Homo sapiens GN=LRRC8C	0	22	28
Kinesin-like protein KIF11 OS=Homo sapiens GN=KIF11	23	24	22
Trypsin OS=Sus scrofa	5	5	6
Keratin, type I cytoskeletal 16 OS=Homo sapiens GN=KRT16	11	20	4
Keratin, type I cytoskeletal 10 OS=Homo sapiens GN=KRT10	14	14	13
Keratin, type II cytoskeletal 2 epidermal OS=Homo sapiens GN=KRT2	9	13	9
Clathrin heavy chain 1 OS=Homo sapiens GN=CLTC	33	0	0
Leucine-rich repeat-containing protein 8B OS=Homo sapiens GN=LRRC8B	0	10	16
Prohibitin-2 OS=Homo sapiens GN=PHB2	9	7	4
Keratin, type II cytoskeletal 6B OS=Homo sapiens GN=KRT6B	6	11	0
Splicing factor 3B subunit 3 OS=Homo sapiens GN=SF3B3	11	8	0
Splicing factor 3B subunit 1 OS=Homo sapiens GN=SF3B1	11	7	0
Prohibitin OS=Homo sapiens GN=PHB	9	7	3
Heterogeneous nuclear ribonucleoproteins C1/C2 OS=Homo sapiens GN=HNRNPC	7	5	0
Keratin, type II cytoskeletal 5 OS=Homo sapiens GN=KRT5	3	6	3
Keratin, type I cytoskeletal 14 OS=Homo sapiens GN=KRT14	2	5	3
Erythrocyte band 7 integral membrane protein OS=Homo sapiens GN=STOM	4	5	4
U2 snRNP-associated SURP motif-containing protein OS=Homo sapiens GN=U2SURP	6	0	0
U5 small nuclear ribonucleoprotein 200 kDa helicase OS=Homo sapiens GN=SNRNP200	8	3	0
Tubulin beta chain OS=Homo sapiens GN=TUBB	3	2	3
Splicing factor 3B subunit 2 OS=Homo sapiens GN=SF3B2	6	3	0
Eukaryotic translation initiation factor 3 subunit A OS=Homo sapiens GN=EIF3A	3	9	0
Pre-mRNA-processing-splicing factor 8 OS=Homo sapiens GN=PRPF8 PE=1 SV=2	9	0	0
Ubiquitin-60S ribosomal protein L40 OS=Homo sapiens GN=UBA52	2	3	3
Ig gamma-1 chain C region, membrane-bound form OS=Mus musculus GN=Ighg1	2	3	3
40S ribosomal protein S8 OS=Homo sapiens GN=RPS8	4	5	0
40S ribosomal protein S3 OS=Homo sapiens GN=RPS3	4	3	0

116 kDa U5 small nuclear ribonucleoprotein component OS=Homo sapiens GN=EFTUD2	6	0	0
Highly divergent homeobox OS=Homo sapiens GN=HDX	0	3	2
40S ribosomal protein S6 OS=Homo sapiens GN=RPS6	3	3	0
Heat shock cognate 71 kDa protein OS=Homo sapiens GN=HSPA8	3	2	2
Nuclease-sensitive element-binding protein 1 OS=Homo sapiens GN=YBX1	2	2	0
40S ribosomal protein S2 OS=Homo sapiens GN=RPS2	2	3	0
Putative pre-mRNA-splicing factor ATP-dependent RNA helicase DHX15 OS=Homo sapiens GN=DHX15	5	0	0
Ig kappa chain C region OS=Mus musculus	0	0	2
Small nuclear ribonucleoprotein Sm D2 OS=Homo sapiens GN=SNRPD2	3	0	0
RNA-binding protein 39 OS=Homo sapiens GN=RBM39	4	2	0
Serine/threonine-protein kinase 38 OS=Homo sapiens GN=STK38	0	0	3
Eukaryotic translation initiation factor 3 subunit B OS=Homo sapiens GN=EIF3B	2	3	0
Matrin-3 OS=Homo sapiens GN=MATR3	3	2	0
Serum albumin OS=Bos taurus GN=ALB	4	0	0
Keratin, type II cytoskeletal 6C OS=Homo sapiens GN=KRT6C	0	2	0
Bcl-2-associated transcription factor 1 OS=Homo sapiens GN=BCLAF1	3	2	0
Calcium homeostasis endoplasmic reticulum protein OS=Homo sapiens GN=CHERP	3	0	0
Small nuclear ribonucleoprotein Sm D3 OS=Homo sapiens GN=SNRPD3	2	0	0
Heterogeneous nuclear ribonucleoprotein U OS=Homo sapiens GN=HNRNPU	0	2	0
Eukaryotic translation initiation factor 3 subunit C OS=Homo sapiens GN=EIF3C	0	2	0
Tubulin alpha-1A chain OS=Homo sapiens GN=TUBA1A	0	0	2
AP-2 complex subunit alpha-1 OS=Homo sapiens GN=AP2A1	2	0	0
40S ribosomal protein S4, X isoform OS=Homo sapiens GN=RPS4X	0	2	0
Keratinocyte-associated transmembrane protein 2 OS=Homo sapiens GN=KCT2	0	0	2
Thyroid hormone receptor-associated protein 3 OS=Homo sapiens GN=THRAP3	2	0	0
40S ribosomal protein S3a OS=Homo sapiens GN=RPS3A	0	3	0
Puromycin-sensitive aminopeptidase OS=Homo sapiens GN=NPEPPS	0	0	2
Pre-mRNA-processing factor 19 OS=Homo sapiens GN=PRPF19	2	0	0
Clathrin heavy chain 1 OS=Oryza sativa subsp. japonica GN=Os11g0104900	2	0	0
AP-2 complex subunit beta OS=Homo sapiens GN=AP2B1	2	0	0
Heterogeneous nuclear ribonucleoprotein K OS=Homo sapiens GN=HNRNPK	2	0	0
RNA-binding protein Raly OS=Homo sapiens GN=RALY	2	0	0
Golgi membrane protein 1 OS=Homo sapiens GN=GOLM1	0	0	2
Pinin OS=Homo sapiens GN=PNN	2	0	0

Table S2: Stable isotope labeled peptides and their multiple reaction monitoring (MRM) transitions. Related to figure 1.

Q1	Q3	RT (min)	Peptide	DP	CE
569.275	773.404	9	LRC8B.SNYSDIPDVK.+2y7.light	72.6	20.4
569.275	686.372	9	LRC8B.SNYSDIPDVK.+2y6.light	72.6	23.4
569.275	458.261	9	LRC8B.SNYSDIPDVK.+2y4.light	72.6	23.4
573.282	781.418	9	LRC8B.SNYSDIPDVK.+2y7.heavy	72.6	20.4
573.282	694.386	9	LRC8B.SNYSDIPDVK.+2y6.heavy	72.6	23.4
573.282	466.275	9	LRC8B.SNYSDIPDVK.+2y4.heavy	72.6	23.4
465.256	816.421	7.9	LRC8A_human.IEQGIVDR.+2y7.light	65	19.6
465.256	687.378	7.9	LRC8A_human.IEQGIVDR.+2y6.light	65	19.6
465.256	559.32	7.9	LRC8A_human.IEQGIVDR.+2y5.light	65	22.6
470.26	826.429	7.9	LRC8A_human.IEQGIVDR.+2y7.heavy	65	19.6
470.26	697.387	7.9	LRC8A_human.IEQGIVDR.+2y6.heavy	65	19.6
470.26	569.328	7.9	LRC8A_human.IEQGIVDR.+2y5.heavy	65	22.6
472.774	743.466	9.3	LRC8C.NSLSVLSPK.+2y7.light	65.6	16.9
472.774	630.382	9.3	LRC8C.NSLSVLSPK.+2y6.light	65.6	19.9
472.774	543.35	9.3	LRC8C.NSLSVLSPK.+2y5.light	65.6	19.9
476.781	751.48	9.3	LRC8C.NSLSVLSPK.+2y7.heavy	65.6	16.9
476.781	638.396	9.3	LRC8C.NSLSVLSPK.+2y6.heavy	65.6	19.9
476.781	551.364	9.3	LRC8C.NSLSVLSPK.+2y5.heavy	65.6	19.9
456.774	670.413	10.2	LRC8D.LELIPEAK.+2y6.light	64.4	16.3
456.774	557.329	10.2	LRC8D.LELIPEAK.+2y5.light	64.4	19.3
456.774	444.245	10.2	LRC8D.LELIPEAK.+2y4.light	64.4	25.3
460.781	678.428	10.2	LRC8D.LELIPEAK.+2y6.heavy	64.4	16.3
460.781	565.344	10.2	LRC8D.LELIPEAK.+2y5.heavy	64.4	19.3
460.781	452.259	10.2	LRC8D.LELIPEAK.+2y4.heavy	64.4	25.3
430.745	718.409	8.7	LRC8E.AATLESLR.+2y6.light	62.5	18.4
430.745	617.362	8.7	LRC8E.AATLESLR.+2y5.light	62.5	21.4
430.745	504.278	8.7	LRC8E.AATLESLR.+2y4.light	62.5	21.4
435.75	728.418	8.7	LRC8E.AATLESLR.+2y6.heavy	62.5	18.4
435.75	627.37	8.7	LRC8E.AATLESLR.+2y5.heavy	62.5	21.4
435.75	514.286	8.7	LRC8E.AATLESLR.+2y4.heavy	62.5	21.4

Table S3: HeLa inducible cell lines with *LRRC8* disrupted. Related to figure 2.

Cell line	Clone name	Genetic alteration
LRRC8(B/D/E)$^{-/-}$	C1	**B**: a1: Δ2nt (c445-t446) a2: Δ1nt (t446)
		D: 1nt insertion (a after c324)
		E: 1nt insertion (a after a94)
LRRC8(B/C/E)$^{-/-}$	D11	**B**: Δ1nt (t446)
		C: a1: Δ5nt (c361-g365) a2: Δ31nt (t346-t376) a3: Δ14nt (c361-a374)
		E: 1nt insertion (a after a94)
LRRC8(B/C/D)$^{-/-}$	E12	**B**: Δ1nt (t446)
		C: 1nt insertion (t after g118)
		D: 1nt insertion (a after c324)
LRRC8(B/C/D/E)$^{-/-}$	E12-13	**B**: Δ1nt (t446)
		C: 1nt insertion (t after g118)
		D: 1nt insertion (a after c324)
		E: 1nt insertion (a after a94)

Table S4: Wildtype HeLa cell lines with *LRRC8* disrupted. Related to figure 3.

Cell line	Clone name	Genetic alteration
LRRC8(B/D/E)$^{-/-}$	BDE9	**B**: 1nt insertion (a after c451)
		D: 1nt insertion (a after c324)
		E: 1nt insertion (a after a94)
LRRC8(B/C/E)$^{-/-}$	BCE8	**B**: 1nt insertion (a after c451)
		C: Δ1nt (c361)
		E: 1nt insertion (a after a94)
LRRC8(B/C/D)$^{-/-}$	BCD4	**B**: 1nt insertion (a after c451)
		C: Δ1nt (c361)
		D: 1nt insertion (a after c324)
LRRC8(A/B/C/D/E)$^{-/-}$	ABCDE9	**A**: a1: 1nt insertion (c after t122) a2: 2nt insertion (cg after t122)
		B: 1nt insertion (a after c451)
		C: Δ1nt (c361)
		D: 1nt insertion (a after c324)
		E: 1nt insertion (a after a94)